# Facile Synthesis of CeO2 Blended CoWO4 Nanocomposites For High Photocatalytic Performance And Investigation of Their Antimicrobial Activity

**S. Selvi**
N.K.R Government Arts College
**N. Jayamani** ( jayamaninataraju@gmail.com )
Government Arts College(Autonomous)
**D. Barathi**
N.K.R Government Arts College

**Research Article**

**Keywords:** CeO2/CoWO4 nanocomposites, Visiblelight, Photodegradation, Methylene blue dye, Recyclability

**Posted Date:** April 27th, 2021

**DOI:** https://doi.org/10.21203/rs.3.rs-439774/v1

# Facile Synthesis of $CeO_2$ blended $CoWO_4$ Nanocomposites for High Photocatalytic Performance and Investigation of their Antimicrobial activity

S. Selvi[a], N. Jayamani[b*], D. Barathi[a]

[a]Department of Physics, N.K.R Government Arts College, Namakkal-637001, Tamilnadu, India.

[b]Department of Physics, Government Arts College(Autonomous), Salem-636001, Tamilnadu, India.

*Email address: jayamaninataraju@gmail.com;

**Abstract**

In this work, novel $CeO_2/CoWO_4$heterostructured nanocomposites (NCs) wassynthesizedvia a hydrothermal method. X-ray diffraction (XRD), high-resolution transmission electron microscopy(HRTEM), UV-VisDRSandphotoluminescence (PL) spectroscopy were categorized herein to gain the crystal structure,deep morphology, optical assets, and charge separation of the as-produced photocatalysts (PCs)respectively. Relatedbythepristine$CoWO_4$,$CeO_2$and $CeO_2/CoWO_4$ photocatalyst was considered by enriched activity of themethylene blue (MB)aqueous dye photodegradation under visible light exposure.Chiefly, the photodegradation efficacy of as-attained$CeO_2/CoWO_4$photocatalystexposed the premierdecomposition ratio (92.5%) of MB dyein105 min among all samples, which was noticeably1.8 and 2.2folds over the pristine $CeO_2$ (43 %) and$CoWO_4$(60 %), separately.Likewise, the $CeO_2/CoWO_4$PCs sustained satisfactory activity even after 4sequentialrecycling runs, signifying its great photocatalytic steadiness and robustness. Hence the ensuingsuperiorPCspreferred the furtherefficient charge ($e^-$-$h^+$) separation, solid visible light fascination,and worthy interfacial energy transfer leads amid$CoWO_4$ and $CeO_2$nanoparticles (NPs).A likely mechanism liable for photodegradation was eventuallyprojected. The synergistic thingsof antibacterialmotionvia$CeO_2/CoWO_4$ NCs were probed by the weld-diffusion scheme.Thus, effortfindingdealswith a novel avenue for the growth of stable and proficientvisible-light active PCs for environmental purification.

**Keywords:** *$CeO_2/CoWO_4$ nanocomposites; Visiblelight; Photodegradation; Methylene blue dye;Recyclability;*

**Introduction**

As photocatalysis deliberatedexistence one of the utmostcapable ways to resolve the growingenvironmental weakening fuel and energy problems,semiconductors (SCs) centeredphotocatalysts(PCs) consumebroadlyfascinatedinto several multidisciplinary domains of materials, environment, chemistry, and copiouscourtesyfor theseverere jection of riskywater toxins(Chowdry et al. 2019; Shu et ak. 2017) Until now, ithas recognized that ecological effluence owed to the speedy industrial and population evolution is a kind of utmost vital tasks facing entire leaving existences in wide-reaching. Still, none of these semiconductor PCs couldcertainlyfulfillfor entiresupplies of realuses, for occurrence, greatexploitation of solar energy, greateffectiveness, high steadiness and low cost (Alshehri et al. 2017; Ke et al. 2018). For case, one of the utmostimperative and low-priced colorants, methylene blue (MB) remainstypicallyused in fabrics as a pigment, photographic and printing trades, also retains the carcinogenic, mutagenic in wildlife,chronic noxiousnessandcould be even bio-accumulate in the food chains towards hominids/animals (Ke et al. 2018; Subhan et al. 2015) . Accordingly, to eliminatethe MB dye since the ecological wastewater byvisible-light-driven photocatalytic progressionstandsanactualcapableand conservationresponsivepolicy to exploit solar energy, togethertoresolve the ecologicaldifficulties (Rashad et al. 2014).Lately, the photocatalytic action of transition metal oxides(TMO)and lanthanideshaveconcerned much kindness toward the requests in the photodegradation of organic poisons inaqueous situations under UV or visible light treatment (Sujatha et al. 2019).

Amidseveral lanthanides, $CeO_2$ nanostructures (NSs)resourceshave fascinated the concern of distinctivepossessionsand the former decade owing to their extensiveclaims in catalysis, gas sensors, ultraviolet ray detectors, and eco-friendly dyestuffs, etc., (Cui et al. 2019; Wetchakun et al. 2012). In $CeO_2$ is a chemically steady oxide nanomaterial, series of its discreteassets such as great optical transparency in the visible province, constancy at high temperature great hardness and proficiency of provided that oxygen species to easy source or relief oxygen alterationamong $Ce^{3+}$ and $Ce^{4+}$ oxidation states of their lattice oxygen assemblyin oxygen vacancies ($V_o$).The cobalt tungstate ($CoWO_4$) as a uniquetransition metal tungstate photocatalyst, retain a narrow band-gappedp-type semiconductor(Eg =~2.8 eV). Sincegreat stability, situationsociability and low-cost assembly, $CoWO_4$ has been used in sensors, colorantessences,supercapacitors, photovoltaic electrochemical cells, and photocatalystdeprivation (Jothivenkatachalam et al. 2015).Yet, owing to the shortefficiency of ($e^-$-$h^+$) separation, the photocatalytic action of pristine $CoWO_4$nanomaterials (NMs)was quite low. As is fine-recognized by agents, the assemblyof heterojunctionassemblyamongSCs couldseriouslyimprove the photocatalytic movement of pristine NMs by refiningtheir charge separation capability and enlargementof the light captivationseries (Ahmadi et al. 2016). Thus, emergingowingPCs by augmentingassetsoverthe pairing, co-catalysts accumulation, fashioningright heterojunction and furtherwas a serious one. It has instantlypreferred to progress the proficient visible-light-driven photocatalyst bymoderatelygreat charge-separation efficacy, also generate photo-carrier traps and diminish the electron-hole ($e^-$-$h^+$) pair recombination rate. To best of our acquaintance, no facts were offered on the combination of $CeO_2$/$CoWO_4$PCs and the consistent application for dyedeductionfor environmental remediation. Hence, construction of $CeO_2$blended in the $CoWO_4$to form $CeO_2$/$CoWO_4$NCswasprobable to attain a high-enactment photocatalyst foraqueous stageMB deletionunder visible light. Later, to overwhelmed the forbidden bandwidth,

relaxed recombination of ($e^-$-$h^+$)pairs and smallconsumption of solar energy to a certain extent, whereas, it couldcaptivatebetter visible light range, great catalytic activity and steadyenactment (Li et al. 2019).

Herein,an existing study, the fruitfulcreation of novel $CeO_2$/$CoWO_4$NCs via superficial hydrothermal chemical is described. These blendsystemsestablishednoble reproducibility and expedited the creation of high-purity yields. The as-equippedPCs revealanintenselyenrichedphotodegradation competence of MB dye. The structural, morphological and opticalassets of $CeO_2$/$CoWO_4$PCs are categorized todeliveranauxiliaryinquiry for the mechanism.The distinctimprovement of photocatalytic motionhasprofitssince theelectron ($e^-$)transferal from $CoWO_4$ into $CeO_2$obsessed by visible-light pitch. The quick($e^-$)injection since $CoWO_4$into $CeO_2$grades in togethera slower recombination rate and extended lifetime of photoexcitedcharges.As follows, this novel $CeO_2$/$CoWO_4$NCsstrategyassistsfurthereffectivesolar energy exploitation of the excited electrons ($e^-$) in $CeO_2$ with engorgedphotocatalytic presentation and antibacterial action.

**Experimental sector**

**Materials**

To perform this revision, Cobaltous nitrate hexahydrate ($Co(NO_3)_3 \cdot 6H_2O$; 99%),Sodium tungstate dihydrate($Na_2WO_4.2H_2O$, 99%), Ethylene glycol (99%) were procured from Himedia Ltd. Potassium chloride (Merck, 99%), Cerium nitrate, ($Ce(NO_3)_3 \cdot 6H_2O$; 98 %)were obtained since SRL Chem.Limited. Sodium hydroxide (NaOH), isopropanol (IPA), Di-sodium Ethylene Diamine Tetra Acetic Acid (EDTA-2Na), benzoquinone (BQ), and absolute ethanol ($CH_3CH_2OH$) were obtained from SDFCL Chemical Reagent Co., Pvt. Ltd. Methylene blue (MB; $C_{16}H_{18}ClN_3S$) dye from SD Fineand was used as received. All the chemicals stayed of analytical/methodical reagent (A.R) grade and used without extrarefinement, deionized water (D.I) was used in wholeinvestigates.

**Preparation of $CeO_2$/$CoWO_4$nanomaterials**

Concisely,0.03 mol of $Ce(NO_3)_3 \cdot 6H_2O$was ultrasonically dissolved in 100 ml of D.I water. $NH_4OH$ was gradually dropped directly into the above solution for pH extended at ~ 12. Lastly, the composed precipitants [8]were kept dryon60 °C for 8 h and extracalcined at 400 °C for 1.5 h to attain $CeO_2$NMs.In thisresearch, the$CeO_2$blended $CoWO_4$NMs,via0.03 mol of $Co(NO_3)_3 \cdot 6H_2O$ and 0.03 mol of $Na_2WO_4.2H_2O$ solutionwas added by 50 ml of D.I water.And 1 mol (50 ml) of $NH_4OH$solution was additional in thepioneer solution, although the pH value wastouched at ~11-12. Afterward, being stirred for 3 h, 0.1 g of as-obtained $CeO_2$NMs was auxiliary added in the upstairsproduces and formerly stirred for 2 h.Then, the reaction mixer was relocatedto heat-treatby160 °C aimed at 24 h in a250 mL Teflon-lined stainless steel autoclave. Finally, the attained$CeO_2$/$CoWO_4$precipitate was obtained through centrifugation andwash awayabundant times viaD.I water and ethanol, promote dried at 65 °C for 8 h, besides, the $CeO_2$/$CoWO_4$ NCs was attained (Yan et al. 2017). Conferring to this scheme, the pristine $CoWO_4$NPs was also attainedviaperformance withoutaccumulation of $CeO_2$NMs.

**Characterization of the as-prepared samples**

Depiction ofall the X-ray diffraction (XRD) pattern wasacquired on anX-ray diffractometer (Rigaku Miniflex-II; X-ray diffractometer) over CuKα radiation.FTIR revisions were done by the Perkin Elmer RX-1 FTIR spectrophotometer. Surface morphologies of as given NMs were scrutinized viahigh resolution scanning electron microscope (HR-SEM; HITACHI S-3000 H) inquiry. The deep morphology,shape and particle size of the sample

were recorded byhigh-resolution transmission electronmicroscopy(HR-TEM)imagesusing JEM-2011; JEOL-Japan. The optical belongingsof the attained samples were considered by a UV-Vis DRS spectrophotometer(UV2550 model, Shimadzu - Japan). The optical absorption of dye degradation samples was performed via a UV-Vis spectrophotometer (UV; Perkin-Elmer Lambda-19).The photoelectron transfer of the catalyst was studied by photoluminescence (PL) spectra on a Perkin-Elmer-LS 45Spectrometerat an excitation sequence of ~ 321 nm.

**Photocatalytic activity of MBdye degradation**

The photodegradationenactment of as-obtained samples (50 mg) was measured by the degradationof MB (20 ppm; 100 mL solution; 10 mg/L) under visible-light exposure(300 W Xe lamp by$\lambda$>420 nm cutoff filter in a Pyrex photocatalytic vessel (Madhan et al. 2015). Preceding toexposure, the suspensions stayedconstant magnetically stirred for around30 min in the dark to certify that the dyesmightextend theabsorption-desorption balance on the photocatalyst superficialand dyes. Successively, the suspension (about 2.5 mL) was minedbycentrifuged each15 min of light irradiation intermission and the attention of composedsolution was exploredvia gauging the concentrated absorbance of MB dye in the peak at ~664 nm. The photodegradation efficacy was extent as resulting formula, Efficiency(%) = $(C_0-C_t)/C_0*100$, wherever$C_0$ and $C_t$exist the UV-visible absorbance spectra rate of dyes solution earlier and afterward destruction.In mature to detect the reactive species caused/trapping mechanismthroughoutthe photocatalytic manner, 1mM of IPA, BQ, and EDTA-2Na were added as quenchers of hydroxyl radicals ($\bullet OH^-$), superoxide radical ($O_2\bullet^-$) and holes ($h^+$) individually (Akbari et al. 2015).

**Antibacterial activity**

To resolvetheantibacterial activity of $CeO_2/CoWO_4$ NCs against pathogenic bacterial strainsviz.Gram-ve ($G^-$)of (*Escherichia coli; E. coli*) and Gram +ve ($G^+$) of (*Staphylococcus aureus; S. aureus)*bacteria,was expert by agar weld diffusion method. The $CeO_2/CoWO_4$ NCs dispersed in DMSO to final concentration solutionswere filtered by Millipore filters for sterilization. The weldimpregnated with 25, 50and 75µg/mLof sample solutions, hencestandard antibiotics DMSO (as negative control) and Ampicillin (positive control) were placed and against the pathogenic bacterial strains on the inoculated agar (Nasir et al. 2017). Antibacterial activity was quantified throughcomputing the distance of circular clear inhibition zones (IZ) on the imperviouscontextual of microbialgrowingafterwardcultivationon 37°C for 36 h in bacterial strains and average values of both assayswere intended also tabularized.

**Results and Discussion**

**XRD analysis**

The crystalline structure and phase purityof as-obtained pristine $CoWO_4$, $CeO_2$, and$CeO_2$/CoWO4NCs are considered by the XRDpattern. As displayed in Figure. 1,the pristine $CoWO_4$sample displaysthespecificXRD diffraction peak of pure monoclinic system,space group P2/aand the transpirepeaks by 2θ values of 18.92°, 23.75°, 36.22°, 53.81° agreeing to the (010), (001), (111), (112) crystal plane of $CoWO_4$ (JCPDS file #15-0867) (Liu et al. 2018). The distinguishing peaks by 2θ values of 28.55°, 32.97°, 47.54°, 56.26°, could be indexed which coincide to (111), (200), (220), (311) crystallographicplanes passionate and well-suited diffraction peaks of cubic phase $CeO_2$(JCPDS file #81-0792) individually (Reddy et al. 2017). The diffraction peak is robust, which designates that it

has a great crystallinity. While the $CeO_2/CoWO_4$ NCsexposed the survival of diffraction peaks of together phases of $CoWO_4$ and $CeO_2$and the diffraction peak liftedtowards aminor angle, signifying that $CeO_2$dropped/occurs in lattice oxygen space, henceforth it indicates that $CeO_2$has activepacking on $CoWO_4$lattice. Peaks interrelated to $CeO_2$/CoWO4 heterojunction NCsarereliable withresultant separate, and no furtherany impurity specific peaks/phasescould benoticedwhich specifyconcurrencethat fruitfulassembly of high purity NCs/hybrid NMs.The average crystallite sizeof pristine $CoWO_4$, $CeO_2$, and$CeO_2/CoWO_4$NCswasdesigned for the most passionate peak since Debye-Scherrer's equation was establish to be 23.5-28,27-30.4 and 25.2-19.05 nm individually. From now,theequation is$D=0.9\lambda/\beta\cos\theta$,whereDstands the crystallite size, λstands fora wavelength of the used X-ray radiation (1.5418A˚),βis the (FWHM)full-width halfmaximumof diffraction peak andθis scattering angle.Since the declined in crystallite size might be expressivelyrepressedowed to the existence of$CoWO_4$ has abundantintegration in the $CeO_2$lattice (Li et al. 2018).

**FTIR spectral analysis**

FTIR analysis was supported to conquer a better visionof the chemical structures, functional groups informationof pristine $CeO_2$, $CoWO_4$ and$CeO_2/CoWO_4$NCsover the frequency range of 4000-400 $cm^{-1}$as revealed in Figure 2. The precise bands at 1045 and 1397 $cm^{-1}$mightthe individual peaks correlated to stretching vibrations kindof C=O and C-O, separately. The typical bandssituatedat 1544 $cm^{-1}$and1625 $cm^{-1}$were consigned to diversetypes of C-H vibration (Jayanthi et al. 2018).The notable bands on 574 $cm^{-1}$were usually recognized owed to the vibrational kind of Ce-O absorption bonding. Likewise, to band realize in the range at 748, 793 and 892 $cm^{-1}$are indorsedto deformation ways of Ce-O-Ce, Co-O and W-O bonds by chains stretching vibrations, individually. The extreme bandsperceived at about 3367and 1548$cm^{-1}$wasowing to O-H stretching vibrationskind(H-bonded)of inside bondedor surface adsorbed hints of residual water ($H_2O$), and the oxygen (O-) functionalitiesindividually (Taneja et al. 2018).

**Surface morphology with the elemental outline**

The surface morphology of as-ascribed pristine $CeO_2$, $CoWO_4$, and $CeO_2/CoWO_4$ NMs samples was resolute by HR-SEMimageries as exposed in Figures 3 (a-c). All the as-obtained samplesdisplayshavevastly agglomerated sphere-like fashionedNSs which were comprised ofthe satisfactoryfoundation ofNPs (Ahmadi et al. 2016; Cui et al. 2018) The elemental purenessCeO2/CoWO4NCs was establishedviathe EDXsystem. As demonstrated in the EDX peaks conforming to theFigure. 3(d), the $CeO_2/CoWO_4$NCs are self-possessed of Ce, W, O, and Co elements. Besides, no furtherimpurity peaks were perceived which specifiespositiveconfiguration (Maddah et al. 2018) with high pureness level of as-obtained $CeO_2/CoWO_4$NCs, and the relative element/contentsweight ratios are indicated in the table (inset Figure. 3(d)).The auxiliary details of the $CeO_2/CoWO_4$heterojunctionNCsarerecognizedthrough EDX mapping, as publicized in Figure. 4. Figure. 4(a)reveals the sample expanse for EDX mapping, illuminating the dispersal of Ce, W, O, and Co elements in Figure.4(a-e). In addition, the Ce, W, O, and Co elements have anidenticalcirculation of the Ce and Oreactive species on the surface/boundary of $CoWO_4$NPs (Pandian et al. 2019).

HRTEM method was used to moresurveyto approvethe features of deepnessmorphology, crystalline nature and particle size of as-obtained NCs. As exposed inFigure 5(a) apparentlyexposesthe high magnification of $CeO_2/CoWO_4$NCs, it was observed that quasi-spherical NPs were noticeablydispersed andaffixedover each other (Alsheri et al. 2017; Cui et al. 2019). The as-organized$CeO_2/CoWO_4$NCsby the average sizesin the range of virtually25-29 nm in attendance of an effective hydrothermal heating manner. Likewise, the selected area electrondiffraction (SAED) outlinesthe inset of Figure. 5(b)exposes that the vibrantlattice fringe fixedmutually, which atteststhegoodconstruction of interfacial assemblyamong $CoWO_4$and $CeO_2$NPs in thecomposites also specifying random directions, whereas it is well-consistent by the XRD outcome. Henceforth it hasfavorable for fact that the photoexcited charge carrier ($e^-$-$h^+$) effortamid the $CeO_2/CoWO_4$NCs (Balavi et al. 2013).

**UV-Vis DRS absorption spectra**

As is well recognized, the photocatalytic action of a photocatalyst is determined via the light absorption capability. Anassessment of the optical absorption possessions for pristine $CeO_2$, $CoWO_4$NPs,and$CeO_2/CoWO_4$NMswasclarifiedby UV-DRS spectrawere revealedin Figure. 6(a). The strong absorption province forecast aboutat 290-400 nm was distinctive of $CeO_2$and $CoWO_4$ NMs. The absorbance edge of pristine $CeO_2$and $CoWO_4$NMssituated at about292 and 295 nmseparately. Withadapting by mixing the $CeO_2/CoWO_4$NCs at the absorbance edges (~296, 465 nm) consume strong visible-light absorptionfurther effectively thanfurther as-obtained NMs, thoughauxiliary red-shifted light absorption capabilitywith great mediate amid$CoWO_4$and $CeO_2$. Theseoutcomespropose that theas-obtained PCs wouldretain visible-light photocatalytic action{Formatting Citation}(Zhao et al. 2018). Toinspect the band-gap energy of as-organizedPCs could be intendedthroughthe Tauc equation byfollowing formula (Prabavathi et al. 2019):$\alpha h\nu = A(h\nu - Eg)^{n/2}$. In the method, αstands for absorption coefficient, hνstands to photon energy, Eg representsthe bandgap, A is a persistent moral relative to the material, individually. The value of n isdecided by the type of optical transition of the semiconductor (i.e., n=1 for directlyallowabletransition and n=4 for indirectlyallowabletransition). Throughconsuming the optical absorption data and this Tauc's equation, the energy gap of pristine $CeO_2$, $CoWO_4$, and$CeO_2/CoWO_4$NCsare 2.92, 2.83 and 2.46 eV, individually (Figure. 6(b)). The bandgap energies weredeclined in composite on mixing of $CeO_2/CoWO_4$, they might be fashionedsince the synergistic influencealso interfacial contactamid $CeO_2$ and $CoWO_4$ NPs leads to the slighter of the bandgapenergysimilarly increasing the visible-light absorptionaptitude(Wang et al. 2018). It was itemized that the well-suitedoverlying band-structure in the composite couldquicken the separation/charge-transfer of electron-hole ($e^-$-$h^+$)sets, thusproposing that $CeO_2/CoWO_4$NCs mightbe refining the photocatalytic motionfor the exclusion of organic impurity under visible light revelation (Pourmasoud et al. 2017).

**Photoluminescence (PL) property**

To categorize the excitation stuff, trapping, charge migration, and separation effectivenessof photo-motivated chargecarriersof the as-attained samples was moreappraisedviaPLemission spectrascrutiny (Yang et al. 2019). The room hotnessPL spectra of the $CeO_2/CoWO_4$heterojunction NCs,pristine $CeO_2$,and$CoWO_4$ NPs were publicized in Figure. 7.Since Figure 7, it was originated that the PL emission intensity of $CeO_2/CoWO_4$was depressed than pristine $CeO_2$and$CoWO_4$ NPs. Speciously the outline of $CoWO_4$NPsindicated a strong emission peak at placed~ 428, 446 and 478 nm, the $CeO_2/CoWO_4$sample exposedknowinglylessened PL intensity, which

expressesthat the heterojunction reservedvia blending with $CeO_2$ and $CoWO_4$ NPs effects in a strangelyhinderedthe recombination rate of photoexcited($e^-$-$h^+$) couples,henceaugmenting the photocatalytic enactment (Singaram et al. 2017). The effectsalso signifying the upgradedcharge separation adeptnessowing to the transference of photoelectrons ($e^-$)across the boundary of $CeO_2$ and $CoWO_4$pairing materials.

**Photocatalytic performance under visible light treatment**

The photocatalytic actions of the as-obtained samples were estimated via the aqueous MB dye photodegradation by visible-light exposure. Figure.8described the consistent UV-Vis absorption spectrum of MB dyephotodegradation with $CeO_2$/$CoWO_4$PCswasrationallyexecuted. In adding, on the $CeO_2$/$CoWO_4$PCs, wasvirtuallyentirely disappeared after the light exposure for 105 min.The pristine $CeO_2$unveiled the minimum photocatalytic action (41 %), and $CoWO_4$as wellexposed a low degradation ratio of around52.5 %. Conversely, the $CeO_2$/$CoWO_4$coupled NCs haveapparentlyenlargedalso an outstanding photocatalytic enactment for MB dye photodegradationwhich is still advanced than other as-obtained samples. After 105 min exposure of visible light, whereasthe $CeO_2$/$CoWO_4$ sample presented the premier photocatalytic action with 92.5 % of dye degraded under the same settings (Feizpoor et al. 2018). The self-degradation/straight photolysisof the dye stoodfewer than 2% after 105 min of light exposure, lateragreeing it to be ignored. The decomposition efficacy of MB dye was projectedby the succeeding expression. Decomposition %=$C_0$−C/$C_0$×100, anywhere $C_0$ and $C_t$are the primary concentration of MB dye andthe equilibrium concentration through the reactionseparately (Wang et al. 2015).The necessity of concentration ratios ($C_t$/$C_0$) on light exposure time is displayed in Figure. 9 (a). The photodegradation proficiency(Figure. 9 (b)) of these catalysts was originated to be in the resultingdirective: $CeO_2$/$CoWO_4$> $CoWO_4$> $CeO_2$. This greater photocatalytic enactment is indorsed to the expressivelyupgraded photoactivity, fortunate photoexcited charge transferences, and light absorption facility of $CeO_2$/$CoWO_4$PCs initiatedvia sensitive influencefor environmental remedying. The heterojunction NCs similarly inhibit the photoexcited($e^-$-$h^+$) recombination, might be recognizedto the developedcharge separation proficiencyamongstthe coupled $CoWO_4$ and $CeO_2$catalytic superficial, and permitting morecapablehabit of the visible light, which henceheightensthe visible-light photocatalytic concert (Priyadharsan et al. 2017).

Additionally, bythe purpose of better compare/defend the photocatalyticdoingsandphotodegradationratekinetics of MB dye consideredover as-inventedsamplessurveyedthe pseudo-first-order kinetic model (Figure. 10 (a)). Also,ln$C_0$/$C_t$=kt, where k symbolized the first-order rate constantplanned from a graph, $C_0$symbolizes the initial attention and $C_t$designates the concentration of MB dye afterward an exposure time t of visible light (Kumar et al. 2016). It has been witnessed that $CeO_2$/$CoWO_4$ PCs have the utmost rate constant of 0.04212 $min^{-1}$, latervirtually3.1, and 1.23 folds advanced than pristine $CeO_2$ (0.0134 $min^{-1}$) and $CoWO_4$ (0.0343 $min^{-1}$) discretely.Agreeing to the outcomes, the photodegradation rate of MB aqueous dyestayedextremelyupgradedowing to the momentousmanipulatingstatistic that the synergistic upshotof coupled $CoWO_4$ and $CeO_2$ NMs existent in the NCs. Upon visibleexposure of $CeO_2$ NPs, the separation of photoelectrons ($e^-$) sinceconduction band (CB) operativerapidlytransported to the $CoWO_4$which aidsto escape/hindering the foundationof photo-motivated($e^-$-$h^+$) pair's recombination andcausing hole ($h^+$) in the valence-band (VB) of $CeO_2$NPsprominent to the improved photocatalytic enactment (Li et al. 2018; Qiao et al. 2018). Lastly, this photo-

excited $e^-$ and $h^+$couldrespond with $H_2O$ to generate$OH^{\bullet-}$ radicals and oxygen species rather than to decay the dye molecules.

**Reusability test**

The reusability and steadinessof photocatalyst NMs are a furtheressentialaspect in real-timeapplications. The succeeding runs of aqueous MB dye over the $CeO_2/CoWO_4$active PCs under visible light were discoveredtoevaluate itsstability trials(Figure. 10 (b)). Respectively cyclic runsrecuperate well again the photocatalyst viacentrifugationwithfurther washed throughD.I water in numeroustimes and dried, hereafter the recovered PCs remainedusedfor the successivecatalytic runs (Zhang et al. 2017).As directed inFigure. 10 (b), there is no deceptivereduction of photodegradation effectiveness during fourreusability paths, likewise,theratio of the effectiveness was faintlydeclined from 92.5 % in the first run to 88 % in the fourth run. Thislessening in photodegradation efficacystaysascribed to the photo-dissolution and photo-corrosion of theas-obtained catalyst. In accumulation, theXRD patterns and FTIR spectra of the $CeO_2/CoWO_4$NC before and after fourrepeated runs were explored in Figure. 11 (A andB).Hence, there was no evidentvarianceamid the intact PCs, establishing that the coupling of $CoWO_4$ and $CeO_2$NMs might availably constrain therecombination of photoexcited ($e^-$-$h^+$) charges to a convinced degree, authorizing the good stability and robustness of $CeO_2/CoWO_4$PCs.Thus, the reusability oftheseoutcomesvalidates that the $CeO_2/CoWO_4$photocatalyst ownsgreat reusable steadiness and prospectivefor practical photocatalytic applications (Magdalane et al. 2017; Yuan et al. 2017 and Zi-ya et al. 2018). Besides, the photodegradation and photoactivity of the $CeO_2/CoWO_4$ catalyst wereequated with several nanocomposite materials (Wei et al. 2014; Rajendran et al. 2016; Hamrouni et al. 2013; Luo et al. 2012; Yang et al. 2012) and it originated in Table. 1.

**Detection of reactive species and the photocatalytic mechanism**

Thatinspectthe photocatalytic mechanisms of $CeO_2/CoWO_4$ heterojunctionphotocatalyst, the dissimilar scavengers were presented to recognize the influences of one or furtherintermediaryreactive/oxidative species ($\bullet OH^-$, $O_2\bullet^-$ and $h^+$) in a photocatalytic manner. As illustratedin Figure. 12, once BQ was added, the degradation competence of MBaqueous colorant was evidentlydeclinedfrom 88.5 % to 23 %, signifying the $^{\bullet}O_2^-$played adynamicpart of active species tophotodegradation (Soltan et al. 2017) . Equally, a momentous loss of photodegradation (45 %), whereasthe adding of IPA, proving the $^{\bullet}OH^-$ pathway influenced a decisive role in the degradation progression. Moreover,whileEDTA-2Na wasadded inaphotocatalytic way, the degradation efficacy of dye was faintly depressed,specifying that littleholes ($h^+$) wereonly involved also it has not a crucialprovider in the photodegradationprogressionof MB dye subtraction. As aneffect, it might be resolved that$^{\bullet}O_2^-$and $^{\bullet}OH^-$were centraldonatedroles of reactive species in the photocatalytic routein visiblelight revelation (Cardillo et al. 2016; Zhu et al. 2018)

On the source of the upstairs experimental grades and the theoretical scrutiny, a projectedenergy band structure illustration of the $CeO_2/CoWO_4$ PCs has established schematically in Figure. 13. The CB and VB edge potential (vs. NHE) (Hao et al. 2017) of $CeO_2/CoWO_4$ PCs at the point of zero charges could be resoluteconsumingMulliken electronegativity equations (1) and (2):

$$E_{VB} = \mathrm{X} - E_e + 0.5\,E_g \rightarrow (1)$$

$$E_{CB} = E_{VB} - E_g \rightarrow (2)$$

Wherever χ is the absolute electronegativity of the semiconductor (χ is 5.56, 6.32 eV for $CeO_2$ and $CoWO_4$, singly). $E_e$stands thefree electron energy of the hydrogen scale (4.5 eV) values and $E_g$ is the bandgap of the obtained semiconductor (Deng et al. 2012). The intended$E_{CB}$ and $E_{VB}$ of $CeO_2$ were -0.40 and 2.52 eV, and of $CoWO_4$ were -0.405 and 3.23 eV, separately. Allowing to UV-DRS results, when the $CeO_2$/$CoWO_4$PCs system was exposed under visible light (>400 nm), together$CeO_2$ and $CoWO_4$ could be stimulated since the energy gap of $CeO_2$ and $CoWO_4$perceived in this revision were 2.92 and 2.83 eV.

To realize the purposeof this enrichment, ananticipated tentative photocatalytic appliance for the photodegradation of MB dye over the $CeO_2$/$CoWO_4$PCs is obtainable in Figure. 13. Since the forgoing inquiry, one couldeffortlesslyinvention that the $CeO_2$ not only plays sustenance but similarlydoings as the ligands, which would be supportive to increase the separation efficacy of photoexcited($e^-$-$h^+$)sets (Liyanage et al. 2014). Linking $CoWO_4$ and $CeO_2$ with different bandgaps to form heterojunction NMs arefurtherflexible than fixing for extending the light absorption and fewerthoughtful to the constituent homogeneity ( García-Pérez et al. 2012; Phanichphant et al. 2016). As visible lightened the surface of $CeO_2$/$CoWO_4$ PCs with adequate energy,$h^+$ and $e^-$ were photoexcited in the VB and CB hereafter be the boundary part series of reactions generating reactive radical species. Yet, photoexcited$h^+$gathered at the VB edge potential of $CoWO_4$ (3.23 eV vs. NHE) respondby $H_2O$ to provide rise to $^{\bullet}OH^-$ radicals, which was the photo-oxidation progressionprominent to expand the charge separation. The photoexcited ($e^-$) at the CB edge potential of $CeO_2$ (-0.40 eV vs. NHE) crystallites are transported to the CB of $CoWO_4$(-0.405 eV vs. NHE) has less negative than the typical redox potential of crystallites. Conversely, the photoexcited($e^-$) on illumined to the CB of $CeO_2$/$CoWO_4$PCs with the adsorbed oxygen softenedin aqueous medium mightease $O_2$to yield$^{\bullet}O_2^-$species (Channei et al. 2015; Sridharan et al. 2019) could respondthrough MB dye and despoiled it into $CO_2$ and $H_2O$. Moreover, these $^{\bullet}O_2^-$ radicals respond with $H_2O$ were contributed in the redox responsefashioned which eventuallycaused $^{\bullet}OH^-$ radicals, and the VB of $h^+$is apprehended by $H_2O$ or respond with a generation of OH groups to form the surface $^{\bullet}OH^-$ radicals which oxidized the dye impurities in visible light. Consequently, centered on the photocatalytic reactivity, the $CeO_2$/$CoWO_4$compositeindicateseffectivesegregation of photoexcited($e^-$-$h^+$)charge-carrier, thus developedphotosensitization and photocatalytic reactivity could be realized positively (Zhang et al. 2018).Theplausiblerepliesconcerningto the upstairs considered substance are invented below [Eqn. 3 to 7].

$$CeO_2/CoWO_4 + Dye + Light \rightarrow CeO_2/CoWO_4 + Dye + (e^-(CB) + h^+(VB)) \rightarrow (3)$$

$$Dye + OH \rightarrow OH^{\cdot -} + Degradation\ \text{Products} \rightarrow (4)$$

$$Dye + O_2 \rightarrow O_2^{-} + \text{Degradation Products} \rightarrow (5)$$

$$Dye + e^-(\text{CB}) \rightarrow \text{Reduction Products} \rightarrow (6)$$

$$Dye + h^+(\text{VB}) \rightarrow \text{Oxidative Products} \rightarrow (7)$$

**Antibacterial accomplishments**

Antibacterial events of $CeO_2$/$CoWO_4$NCs were partitioned against pathogenic bacterial strains, for instance, $G^-$ of *E. coli* and $G^+$ of *S. aureus*bacteria, was proficientby the agar well diffusion system. Figure. 14visibly shows the zoneof inhibition (ZOI) by different concentrations (25, 50and 100 µg/mL) of $CeO_2$/$CoWO_4$,$CoWO_4$, and

$CeO_2$with respect to the typical control which directed the antibacterial outcome. Antibacterial action of as-obtained catalystson the pathogenic bacterial strains by different attention is publicized in Table 2. The superiorantibacterial doings of the as-attained $CeO_2/CoWO_4$NCs onthe concentration of 75µg/mLconsumed a capable antibacterial influencebesideG$^+$ of *S. aureus*bacteriathrough a ZOI value of ~6.5-9 mm on equatingby the typical drug, DMSO (as negative control). Moreover, the united $CoWO_4/CeO_2$was obviouslyindicated that the NCs collectedround the surface membranes, which mightrespond with the microbial membranes and produced internalization of the NCs in the microbe's cells (Magdalane et al. 2016). The mechanism for the bactericidal motion of NPs appearancessubstantialefficacy for the responsive/reactive oxygen species (ROS) and its bactericidalstrains actualpart in its metallic NPs and their complexesin the existenceof oxygen species and accordingly (Gasmalla et al. 2019), donate to the superior mechanical damage for the utilities of microbes, and enriched bactericidal influence of unified$CoWO_4/CeO_2$nanostructured materials.Moreover, thegreaterattentiveness of all these managed NCs materials are destructive to together the consumers and microorganisms, but still, nano-level attention of these NMs are further applications for the destruction of microbes (Sundaram et al. 2017).

**Conclusion**

In summary, a novel $CeO_2/CoWO_4$heterostructured NCs photocatalyst was effectivelydeveloped through a facile hydrothermal assisted process. The assembly of effective NCswas categorizedthrough XRD, HRTEM, UV-DRS, PL spectra, andphotocatalytic revisions. The $CeO_2/CoWO_4$NCs byagglomeration virtually sphericalfashioned morphology with an average size of almost25-29 nm, likewiserevealedadmirable optical belongings and energy bandgap value of 2.46eV. The photocatalytic test of $CeO_2/CoWO_4$PCsindicatedobservablymuch superior photodegradationefficacybeside an aqueous MB dye solutioni.e. 92.5 % within 105 mininvisible light coverageequated togethertheCoWO$_4$ and $CeO_2$ NPs. Additionally, the $CeO_2/CoWO_4$PCs confirmed good recyclability and high steadinessduring four recyclinghenceforthcould be reprocessed.The enriched photoactivity of $CeO_2/CoWO_4$PCscould be renownedto the upsurge in light-harvesting proficiency, actual transfer, andseparation of photoexcited($e^-$-$h^+$)setsowingto proper energy band potentials amidthe synergistic influenceinto the interfaceof CoWO$_4$ and $CeO_2$ NPs. The $^{\bullet}O_2^-$and $^{\bullet}OH^-$ were account for the effectualreactive speciesto removal and mineralization throughthe degradation manner.The feasible mechanism behind in the photodegradationof MB dye in attendanceof $CeO_2/CoWO_4$PCs was eventuallydefined. Likewise, the synthesized $CeO_2/CoWO_4$NCs expression the momentousinfluence on the antibacterial actions against pathogenic bacterial strains. This exertion mightaccessible a newcapable platform for the well-ordered stable $CeO_2/CoWO_4$heterostructured PCswith facilitatesgreatefficientsolar energy conversionto resolve the basic environment concernsaccompanying water effluence remediation.

**Compliance with ethical standards**

**Conflict of interest** The authors state that their research has no interest or financial conflicts of interest.

**Ethical standard** No studies or animal experiments are conducted in this article by any of the authors.

**Informed consent** This article is entirely unprotected as far as patient care is concerned.

**References:**


Ahmadi F, Rahimi-Nasrabadi M, Fosooni A, Daneshmand M (2016) Synthesis and application of $CoWO_4$ nanoparticles for degradation of methyl orange. J Mater Sci Mater Electron 27:9514–9519. https://doi.org/10.1007/s10854-016-5002-7

Akbari-Fakhrabadi A, Saravanan R, Jamshidijam M, et al (2015) Preparation of nanosized yttrium doped $CeO_2$ catalyst used for photocatalytic application. J Saudi Chem Soc 19:505–510. https://doi.org/10.1016/j.jscs.2015.06.003

Alshehri SM, Ahmed J, Alzahrani AM, Ahamad T (2017) Synthesis, characterization, and enhanced photocatalytic properties of $NiWO_4$ nanobricks. New J Chem 41:8178–8186. https://doi.org/10.1039/c7nj02085f

Balavi H, Samadanian-Isfahani S, Mehrabani-Zeinabad M, Edrissi M (2013) Preparation and optimization of $CeO_2$ nanoparticles and its application in photocatalytic degradation of Reactive Orange 16 dye. Powder Technol 249:549–555. https://doi.org/10.1016/j.powtec.2013.09.021

Cardillo D, Weiss M, Tehei M, et al (2016) Multifunctional $Fe_2O_3/CeO_2$ nanocomposites for free radical scavenging ultraviolet protection. RSC Adv 6:65397–65402. https://doi.org/10.1039/c6ra10951a

Channei D, Inceesungvorn B, Wetchakun N, et al (2014) Photocatalytic degradation of methyl orange by $CeO_2$ and Fe-doped CeO2 films under visible light irradiation. Sci Rep 4:. https://doi.org/10.1038/srep05757

Cui H, Li B, Zhang Y, et al (2018) Constructing Z-scheme based $CoWO_4$/CdS photocatalysts with enhanced dye degradation and H2 generation performance. Int J Hydrogen Energy 43:18242–18252. https://doi.org/10.1016/j.ijhydene.2018.08.050

Cui Z, Zhou H, Wang G, et al (2019) Enhancement of the visible-light photocatalytic activity of $CeO_2$ by chemisorbed oxygen in the selective oxidation of benzyl alcohol. New J Chem 43:7355–7362. https://doi.org/10.1039/c9nj01098j

Deng J, Chang L, Wang P, et al (2012) Preparation and magnetic properties of $CoWO_4$ nanocrystals. Cryst Res Technol 47:1004–1007. https://doi.org/10.1002/crat.201200130

Feizpoor S, Habibi-Yangjeh A (2018) Ternary $TiO_2/Fe_3O_4/CoWO_4$ nanocomposites: Novel magnetic visible-light-driven photocatalysts with substantially enhanced activity through p-n heterojunction. J Colloid Interface Sci 524:325–336. https://doi.org/10.1016/j.jcis.2018.03.069

García-Pérez UM, Martínez-De La Cruz A, Peral J (2012) Transition metal tungstates synthesized by co-precipitation method: Basic photocatalytic properties. Electrochim Acta 81:227–232. https://doi.org/10.1016/j.electacta.2012.07.045

Gasmalla HB, Lu X, Shinger MI, et al (2019) Novel magnetically separable of $Fe_3O_4$ /$Ag_3PO_4$@$WO_3$ nanocomposites for enhanced photocatalytic and antibacterial activity against Staphylococcus aureus (S. aureus). J Nanobiotechnology 17:1–14. https://doi.org/10.1186/s12951-019-0485-z

Hamrouni A, Lachheb H, Houas A (2013) Synthesis, characterization and photocatalytic activity of ZnO-$SnO_2$ nanocomposites. Mater Sci Eng B Solid-State Mater Adv Technol 178:1371–1379. https://doi.org/10.1016/j.mseb.2013.08.008

Hao X, Jin Z, Yang H, et al (2017) Peculiar synergetic effect of $MoS_2$ quantum dots and graphene on Metal-Organic Frameworks for photocatalytic hydrogen evolution. Appl Catal B Environ 210:45–56. https://doi.org/10.1016/j.apcatb.2017.03.057

Jayanthi M, Lavanya T, Saradha NA, et al (2017) Superior Photocatalytic Performance of $CeO_2$ Nanoparticles and Reduced Graphene Oxide Nanocomposite Prepared by Low Cost Co-Precipitation Method . J Nanosci Nanotechnol 18:3257–3265. https://doi.org/10.1166/jnn.2018.14701

Jothivenkatachalam K, Prabhu S, Nithya A, et al (2015) Solar, visible and UV light photocatalytic activity of $CoWO_4$ for the decolourization of methyl orange. Desalin Water Treat 54:3134–3145. https://doi.org/10.1080/19443994.2014.906324

Karuppiah S, Thangaraj S, Palaniappan SA, Lakshmanan SO (2019) Influence of surfactants on structural, morphological, optical and antibacterial properties of $SnO_2$ nanoparticles. IET Nanobiotechnology 13:952–956. https://doi.org/10.1049/iet-nbt.2019.0095

Ke J, Adnan Younis M, Kong Y, et al (2018) Nanostructured Ternary Metal Tungstate-Based Photocatalysts for Environmental Purification and Solar Water Splitting: A Review. Nano-Micro Lett 10:. https://doi.org/10.1007/s40820-018-0222-4

Kumar S, Ojha AK (2016) Ni, Co and Ni-Co codoping induced modification in shape, optical band gap and enhanced photocatalytic activity of $CeO_2$ nanostructures for photodegradation of methylene blue dye under visible light irradiation. RSC Adv 6:8651–8660. https://doi.org/10.1039/c5ra14184b

Li S, Hu S, Jiang W, et al (2018) Facile synthesis of cerium oxide nanoparticles decorated flower-like bismuth molybdate for enhanced photocatalytic activity toward organic pollutant degradation. J Colloid Interface Sci 530:171–178. https://doi.org/10.1016/j.jcis.2018.06.084

Li Z, Liu D, Huang W, et al (2019) Applying facilely synthesized $CuO/CeO_2$ photocatalyst to accelerate methylene blue degradation in hypersaline wastewater. Surf Interface Anal 51:336–344. https://doi.org/10.1002/sia.6585

Liu Z, Xu J, Li Y, Yu H (2018) High Performance Photocatalytic Based on Ce Doped $CoWO_4$: Controllable Synthesis and Enhanced Photocatalytic Activity. Catal Letters 148:3205–3213. https://doi.org/10.1007/s10562-018-2518-x

Luo Q, Yu X, Lei B, et al (2012) J. Phys. Chem. C 2012, 116, 8111−8117.PDF. 8111–8117

Maddah B, Jookar-Kashi F, Akbari M (2018) Facile precipitation synthesis of pure $Fe_3O_4/CoWO_4$ nanocomposites and investigation of their photocatalyst and antimicrobial activity. J Mater Sci Mater Electron 29:13723–13730. https://doi.org/10.1007/s10854-018-9502-5

Madhan D, Rajkumar P, Rajeshwaran P, et al (2015) One-step synthesis, characterization, and visible light photocatalytic activity of pure and Zn-doped $SnO_2$ nanoparticles. Appl Phys A Mater Sci Process 120:463–469. https://doi.org/10.1007/s00339-015-9240-y

Magdalane CM, Kaviyarasu K, Vijaya JJ, et al (2016) Photocatalytic activity of binary metal oxide nanocomposites of $CeO_2$/CdO nanospheres: Investigation of optical and antimicrobial activity. J Photochem Photobiol B Biol 163:77–86. https://doi.org/10.1016/j.jphotobiol.2016.08.013

Magdalane CM, Kaviyarasu K, Vijaya JJ, et al (2017) Evaluation on the heterostructured $CeO_2/Y_2O_3$ binary metal oxide nanocomposites for UV/Vis light induced photocatalytic degradation of Rhodamine - B dye for textile engineering application. J Alloys Compd 727:1324–1337. https://doi.org/10.1016/j.jallcom.2017.08.209

Nanorods C, Liyanage AD, Perera SD, et al (2014) Synthesis, Characterization, and Photocatalytic Activity of Y - Doped $CeO_2$ Nanorods

Nasir Z, Shakir ML, Wahab R, et al (2017) Co-precipitation synthesis and characterization of Co doped $SnO_2$ NPs, HSA interaction via various spectroscopic techniques and their antimicrobial and photocatalytic activities. Int J Biol Macromol 94:554–565. https://doi.org/10.1016/j.ijbiomac.2016.10.057

Pandiyan R, Mahalingam S, Ahn YH (2019) Antibacterial and photocatalytic activity of hydrothermally synthesized $SnO_2$ doped GO and CNT under visible light irradiation. J Photochem Photobiol B Biol 191:18–25. https://doi.org/10.1016/j.jphotobiol.2018.12.007

Sundaram IM, Kalimuthu S, Ponniah GP (2017) Highly active ZnO modified g-$C_3N_4$ Nanocomposite for dye degradation under UV and Visible Light with enhanced stability and antimicrobial activity. Compos Commun 5:64–71. https://doi.org/10.1016/j.coco.2017.07.003

Paul Chowdhury A, Shambharkar BH (2020) Synthesis and characterization of BiOCl-$CoWO_4$ nanocomposites with improved photocatalytic activity

Phanichphant S, Nakaruk A, Channei D (2016) Photocatalytic activity of the binary composite $CeO_2$ /$SiO_2$ for degradation of dye. Appl Surf Sci 387:214–220. https://doi.org/10.1016/j.apsusc.2016.06.072

Pourmasoud S, Eghbali-Arani M, Ahmadi F, Rahimi-Nasrabadi M (2017) Synthesis, characterization, and morphological control of $PbWO_4$ nanostructures through precipitation method and its photocatalyst application. J Mater Sci Mater Electron 28:17089–17097. https://doi.org/10.1007/s10854-017-7635-6

Prabavathi SL, Govindan K, Saravanakumar K, et al (2019) Construction of heterostructure $CoWO_4$/g-$C_3N_4$ nanocomposite as an efficient visible-light photocatalyst for norfloxacin degradation. J Ind Eng Chem. https://doi.org/10.1016/j.jiec.2019.08.035

Priyadharsan A, Vasanthakumar V, Karthikeyan S, et al (2017) Multi-functional properties of ternary $CeO_2$/$SnO_2$/rGO nanocomposites: Visible light driven photocatalyst and heavy metal removal. J Photochem Photobiol A Chem 346:32–45. https://doi.org/10.1016/j.jphotochem.2017.05.030

Qiao Q, Yang K, Ma L, et al Facile in situ construction of mediator- free direct Z-scheme g-$C_3N_4$ /$CeO_2$ heterojunctions with highly efficient photocatalytic activity

Rajendran S, Khan MM, Gracia F, et al (2016) $Ce^{3+}$-ion-induced visible-light photocatalytic degradation and electrochemical activity of ZnO/$CeO_2$ nanocomposite. Sci Rep 6:1–11. https://doi.org/10.1038/srep31641

Rashad MM, Ismail AA, Osama I, et al (2014) Photocatalytic decomposition of dyes using ZnO doped $SnO_2$ nanoparticles prepared by solvothermal method. Arab J Chem 7:71–77. https://doi.org/10.1016/j.arabjc.2013.08.016

Reddy Yadav LS, Lingaraju K, Daruka Prasad B, et al (2017) Synthesis of $CeO_2$ nanoparticles: Photocatalytic and antibacterial activities. Eur Phys J Plus 132:. https://doi.org/10.1140/epjp/i2017-11462-4

Shu Z, Zhang Y, Ouyang J, Yang H (2017) Characterization and synergetic antibacterial properties of ZnO and $CeO_2$ supported by halloysite. Appl Surf Sci 420:833–838. https://doi.org/10.1016/j.apsusc.2017.05.219

Singaram B, Varadharajan K, Jeyaram J, et al (2017) Preparation of cerium and sulfur codoped $TiO_2$ nanoparticles based photocatalytic activity with enhanced visible light. J Photochem Photobiol A Chem 349:91–99. https://doi.org/10.1016/j.jphotochem.2017.09.003

Soltan W Ben, Lassoued MS, Ammar S, Toupance T (2017) Vanadium doped $SnO_2$ nanoparticles for photocatalytic degradation of methylene blue. J Mater Sci Mater Electron 28:15826–15834. https://doi.org/10.1007/s10854-017-7477-2

Sridharan M, Kamaraj P, Huh YS, et al (2019) Quaternary CZTS nanoparticle decorated $CeO_2$ as a noble metal free p-n heterojunction photocatalyst for efficient hydrogen evolution. Catal Sci Technol 9:3686–3696. https://doi.org/10.1039/c9cy00429g

Subhan MA, Ahmed T, Uddin N, et al (2015) Synthesis, characterization, PL properties, photocatalytic and antibacterial activities of nano multi-metal oxide $NiO{\cdot}CeO_2{\cdot}ZnO$. Spectrochim Acta - Part A Mol Biomol Spectrosc 136:824–831. https://doi.org/10.1016/j.saa.2014.09.100

Taneja P, Sharma S, Umar A, et al (2018) Visible-light driven photocatalytic degradation of brilliant green dye based on cobalt tungstate ($CoWO_4$) nanoparticles. Mater Chem Phys 211:335–342. https://doi.org/10.1016/j.matchemphys.2018.02.041

Wang L, Ding J, Chai Y, et al (2015) $CeO_2$ nanorod/g-$C_3N_4$/N-rGO composite: enhanced visible-light-driven photocatalytic performance and the role of N-rGO as electronic transfer media. Dalt Trans 44:11223–11234. https://doi.org/10.1039/c5dt01479d

Wang X, Su W, Hu X, et al (2019) Synthesis and characterization of Fe-doped $CdWO_4$ nanoparticles with enhanced photocatalytic activity. Mater Res Express 6:1–9. https://doi.org/10.1088/2053-1591/aaf432

Wei H, Wang L, Li Z, et al (2011) Synthesis and Photocatalytic Activity of One-Dimensional CdS@$TiO_2$ Core-Shell Heterostructures. Nano-Micro Lett 3:6–11. https://doi.org/10.1007/bf03353645

Wetchakun N, Chaiwichain S, Inceesungvorn B, et al (2012) $BiVO_4$/$CeO_2$ nanocomposites with high visible-light-induced photocatalytic activity. ACS Appl Mater Interfaces 4:3718–3723. https://doi.org/10.1021/am300812n

Yan X, Wu Z, Huang C, et al (2017) Hydrothermal synthesis of CdS/$CoWO_4$ heterojunctions with enhanced visible light properties toward organic pollutants degradation. Ceram Int 43:5388–5395. https://doi.org/10.1016/j.ceramint.2016.12.060

Yang G, Yan Z, Xiao T (2012) Preparation and characterization of SnO 2 /ZnO/$TiO_2$ composite semiconductor with enhanced photocatalytic activity. Appl Surf Sci 258:8704–8712. https://doi.org/10.1016/j.apsusc.2012.05.078

Yang H, Xu B, Yuan S, et al (2019) Synthesis of Y-doped $CeO_2$/PCN nanocomposited photocatalyst with promoted photoredox performance. Appl Catal B Environ 243:513–521. https://doi.org/10.1016/j.apcatb.2018.10.057

Yuan Y, Huang GF, Hu WY, et al (2017) Construction of g-$C_3N_4$/$CeO_2$/ZnO ternary photocatalysts with enhanced photocatalytic performance. J Phys Chem Solids 106:1–9. https://doi.org/10.1016/j.jpcs.2017.02.015

Zhang H, Tian W, Li Y, et al (2018) Heterostructured $WO_3$@$CoWO_4$ bilayer nanosheets for enhanced visible-light photo, electro and photoelectro-chemical oxidation of water. J Mater Chem A 6:6265–6272. https://doi.org/10.1039/c8ta00555a

Zhang J, Peng LL, Tang Y, Wu H (2017) Convenient synthesis of twin-Christmas tree-like $PbWO_4$ microcrystals and their photocatalytic properties. Front Mater Sci 11:139–146. https://doi.org/10.1007/s11706-017-0381-0

Zhao Y, Chen T, Ma R, et al (2018) Synthesis of flower-like $CeO_2$/BiOCl heterostructures with enhanced ultraviolet light photocatalytic activity. Micro Nano Lett 13:1394–1398. https://doi.org/10.1049/mnl.2018.5228

Zhu L, Li H, Liu Z, et al (2018) Synthesis of the 0D/3D CuO/ZnO Heterojunction with Enhanced Photocatalytic Activity. J Phys Chem C 122:9531–9539. https://doi.org/10.1021/acs.jpcc.8b01933

Zi-ya L, Man-ying Z, Jing-ling W (2018) Enhanced Visible-Light Photocatalytic and Antibacterial Activities of Ag-Doped g-$C_3N_4$ Nanocomposites. ChemistrySelect 3:10630–10636. https://doi.org/10.1002/slct.201802287

**Table 1.** Comparison of visible light assisted MB photodegradation rate (%) over of previously reported nanomaterials

| **S. No** | **Catalyst** | **Irradiation time (min)** | **Degradation Efficiency (%)** | **References** |
|---|---|---|---|---|
| 1. | $CdS/TiO_2$ | 310 | 62 | Rei et al. 2014 |
| 2. | CeO/ZnO | 150 | 97 | Rajendran et al. 2016 |
| 3. | $ZnO/SnO_2$ | 240 | 100 | Hamrouni et al. 2013 |
| 4. | rGO/ZnO | 90 | 99 | Luo et al. 2012 |
| 5. | $SnO_2/ZnO/TiO_2$ | 300 | 27 | Yang et al. 2012 |
| 6. | $CeO_2$-$CoWO_4$ | 105 | 92.5 % | **This work** |

**Table 2.** Assessment on the zone of inhibition of antibacterial activity for as-prepared nanoparticles.

| S. No. | Microorganisms | Zone of inhibition range (mm) | | | | | |
|---|---|---|---|---|---|---|---|
| | | *E. Coli* | | | *S. aureus* | | |
| | | *25* µg | *50* µg | *75* µg | *25* µg | *50* µg | *75* µg |
| 1 | $CeO_2$ | 2 ± 0.5 | 2.5 ± 1 | 3.5 ± 0.5 | 3 ± 1 | 6 ± 1 | 7 ± 1 |
| 2 | $CoWO_4$ | 2 ± 1 | 2 ± 0.5 | 3 ± 0.3 | 3.5 ± 1 | 6.5 ± 0.5 | 8.5 ± 0.5 |
| 3 | $CeO_2$-$CoWO_4$ | 3.5 ± 0.5 | 3.5 ± 0.5 | 4 ± 1.5 | 6.5 ± 0.5 | 8 ± 0.5 | 11 ± 0.5 |

**Figure caption:**

**Figure 1.** XRD pattern of (a) $CeO_2$ (b) $CoWO_4$ and (c) $CeO_2/CoWO_4$ NCs

**Figure 2.** FTIR spectra of (a) $CeO_2$ (b) $CoWO_4$ and (c) $CeO_2/CoWO_4$ NCs

**Figure 3.** HR-SEM images of (a) $CeO_2$ (b) $CoWO_4$ (c) $CeO_2/CoWO_4$ and (d) EDAX spectra of $CeO_2/CoWO_4$ NCs

**Figure 4.** Elemental mapping of $CeO_2/CoWO_4$ NCs

**Figure. 5** HR-TEM images of as-obtained $CeO_2/CoWO_4$ NCs

**Figure 6.** UV-Vis DRS spectra and (inset) Band gap energy of as-obtained nanomaterials

**Figure 7.** Room-temperature PL spectra of as-obtained nanomaterials

**Figure 8.** UV-Vis absorption spectra of MB dye degradation of $CeO_2/CoWO_4$ NCs

**Figure 9.** Photodegradation of MB dye over the (a) $CeO_2$ (b) $CoWO_4$ (c) $CeO_2/CoWO_4$ PCs

**Figure 10.** Degradation efficiency of MB dye by (a) $CeO_2$ (b) $CoWO_4$ (c) $CeO_2/CoWO_4$ PCs

**Figure 11.** First-order kinetic plot for the degradation of MB over the as-obtained PCs

**Figure 12.** Four repetitive recycling processes of $CeO_2/CoWO_4$ PCs for photodegradation of MB dye under visible light exposure

**Figure 13.** (A) XRD pattern and (B) FTIR spectra for $CeO_2/CoWO_4$ PCs before and after a photocatalytic reaction

**Figure 14.** Effects of different scavengers on the degradation of MB dye in the presence of $CeO_2/CoWO_4$ PCs

**Figure 15**. The plausible mechanism of the MB dye degradation for $CeO_2/CoWO_4$ PCs

**Figure. 16** Antibacterial ZOI value by ($G^-$) *E. coli* and ($G^+$) of *S. aureus* bacteria of *75* µg as-prepared $CeO_2/CoWO_4$ nanomaterials

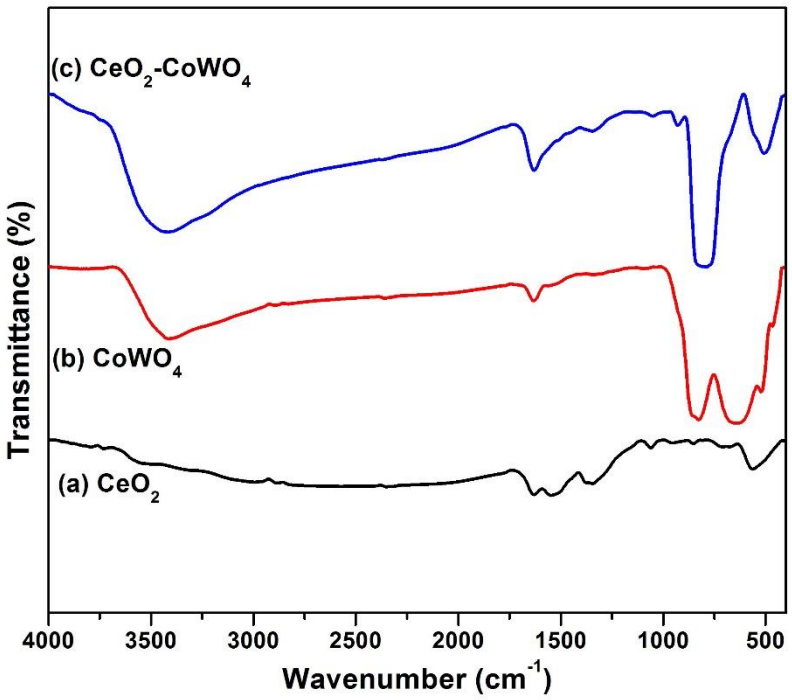
(c) CeO2-CoWO4
(b) CoWO4
(a) CeO2
Transmittance (%)
4000
3500
3000
2500
2000
1500
1000
500
Wavenumber (cm-1)

**Fig. 1**

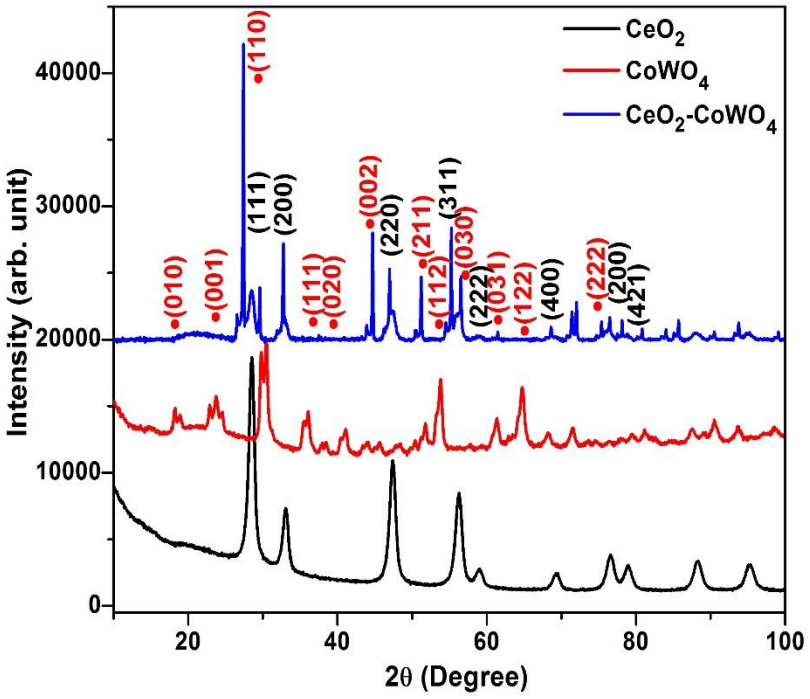
CeO2
CoWO4
CeO2-CoWO4
Intensity (arb. unit)
2θ (Degree)
(010)
(001)
(110)
(111)
(200)
(111)
(020)
(002)
(220)
(211)
(112)
(311)
(030)
(222)
(031)
(122)
(400)
(222)
(200)
(421)

**Fig.2**

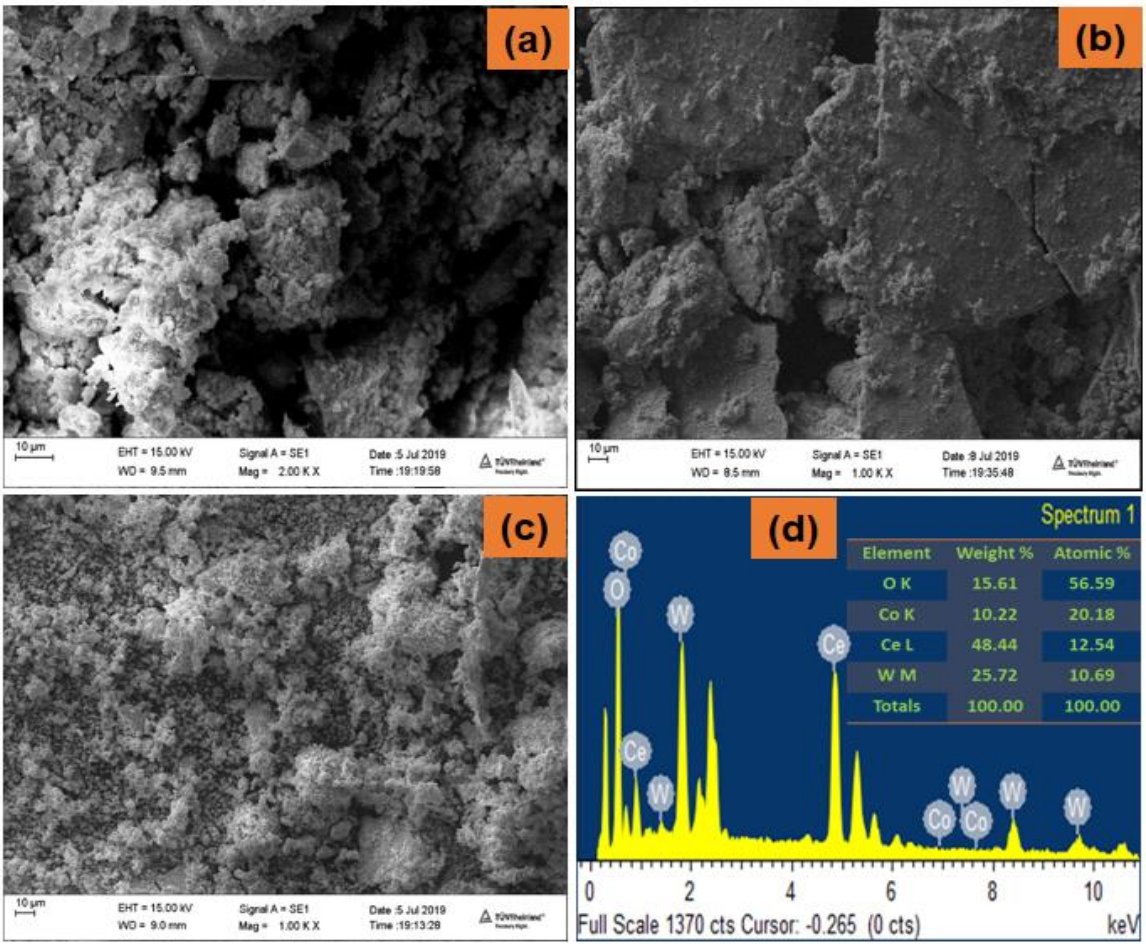
(a)
10 µm
EHT = 15.00 kV
WD = 9.5 mm
Signal A = SE1
Mag = 2.00 K X
Date :5 Jul 2019
Time :19:19:58
(b)
10 µm
EHT = 15.00 kV
WD = 8.5 mm
Signal A = SE1
Mag = 1.00 K X
Date :8 Jul 2019
Time :19:35:48
(c)
10 µm
EHT = 15.00 kV
WD = 9.0 mm
Signal A = SE1
Mag = 1.00 K X
Date :5 Jul 2019
Time :19:13:28
(d)
Spectrum 1
Element | Weight % | Atomic %
O K | 15.61 | 56.59
Co K | 10.22 | 20.18
Ce L | 48.44 | 12.54
W M | 25.72 | 10.69
Totals | 100.00 | 100.00
Co
O
W
Ce
Ce
W
W
Co
Co
W
W
0
2
4
6
8
10
Full Scale 1370 cts Cursor: -0.265 (0 cts)
keV

**Fig. 3**

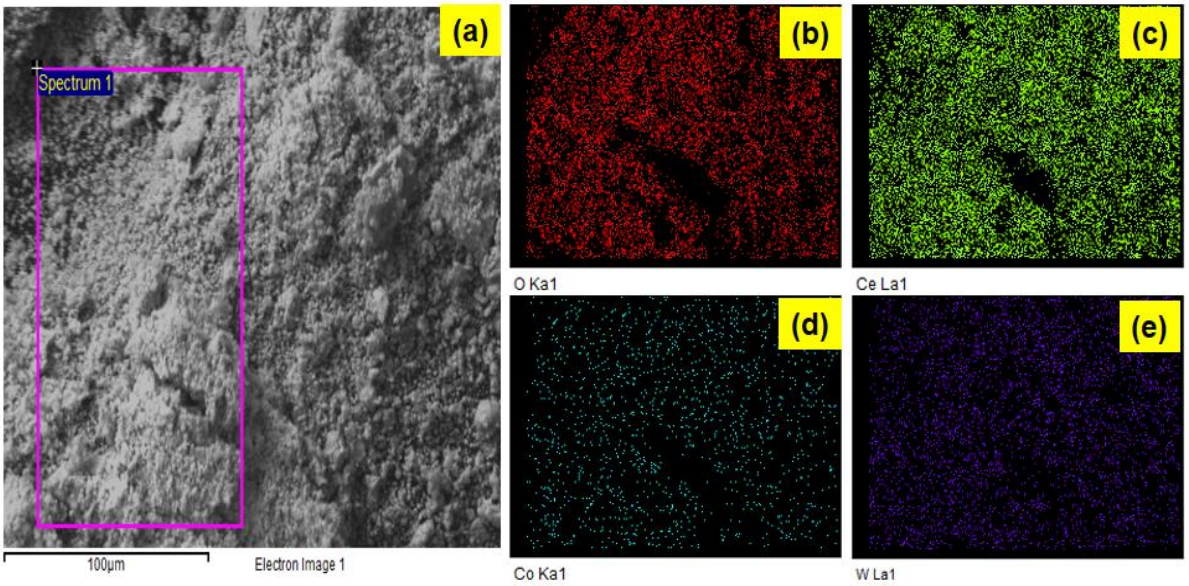
(a)
Spectrum 1
100µm
Electron Image 1
(b)
O Ka1
(c)
Ce La1
(d)
Co Ka1
(e)
W La1

**Fig. 4**

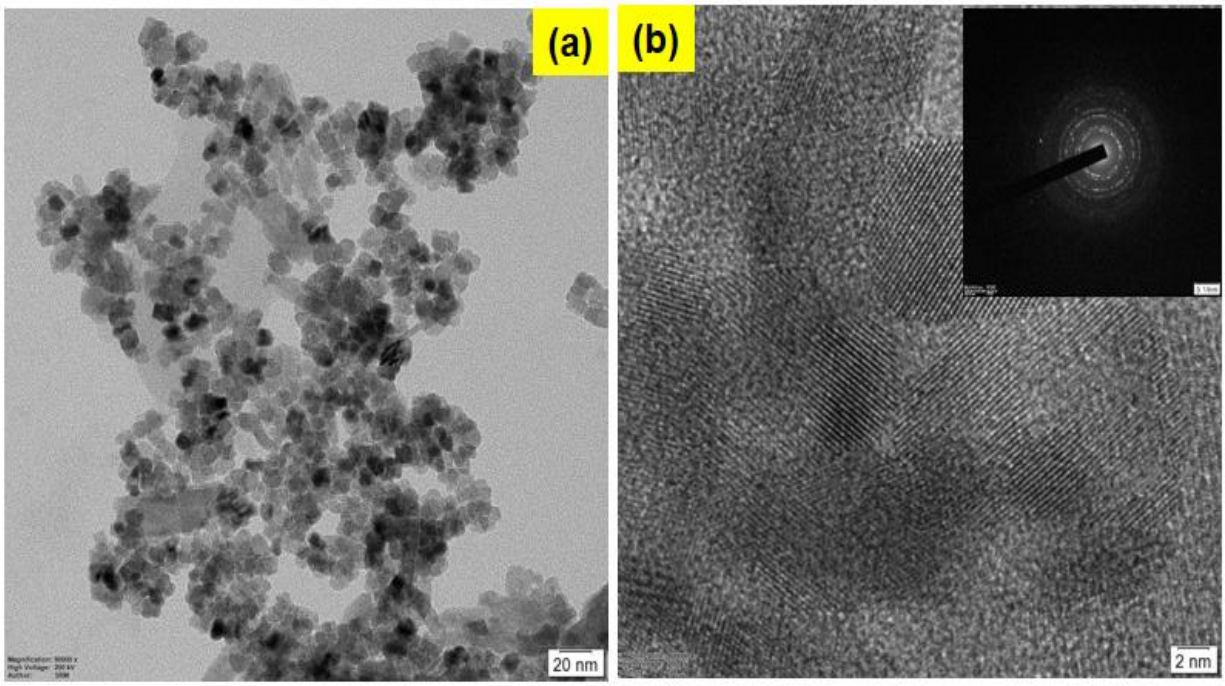


**Fig. 5**

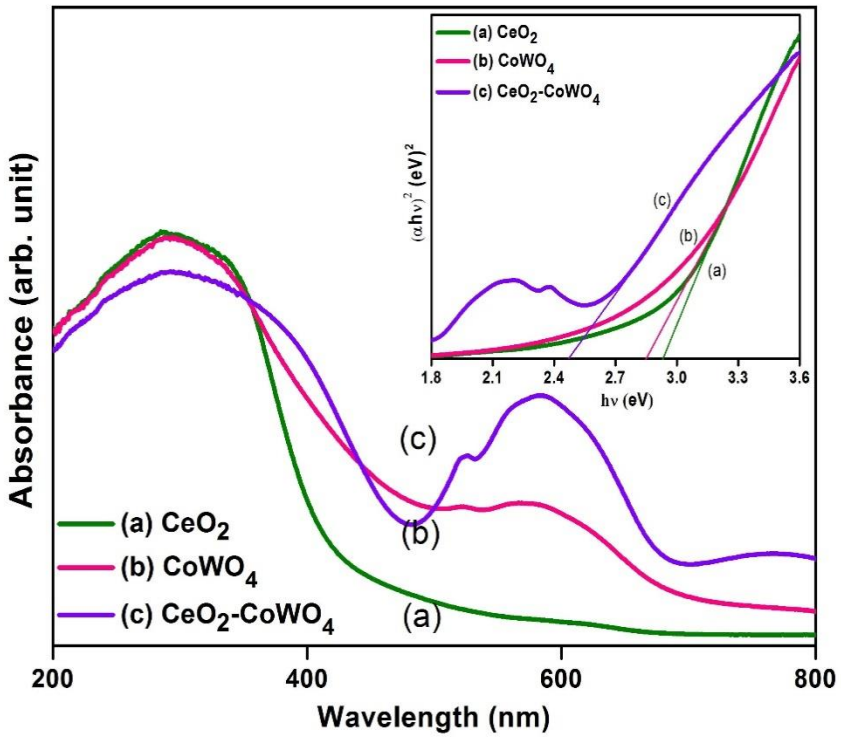
Absorbance (arb. unit)
Wavelength (nm)
200
400
600
800
(a) CeO2
(b) CoWO4
(c) CeO2-CoWO4
(a)
(b)
(c)
(αhν)2 (eV)2
hν (eV)
1.8
2.1
2.4
2.7
3.0
3.3
3.6

**Fig. 6**

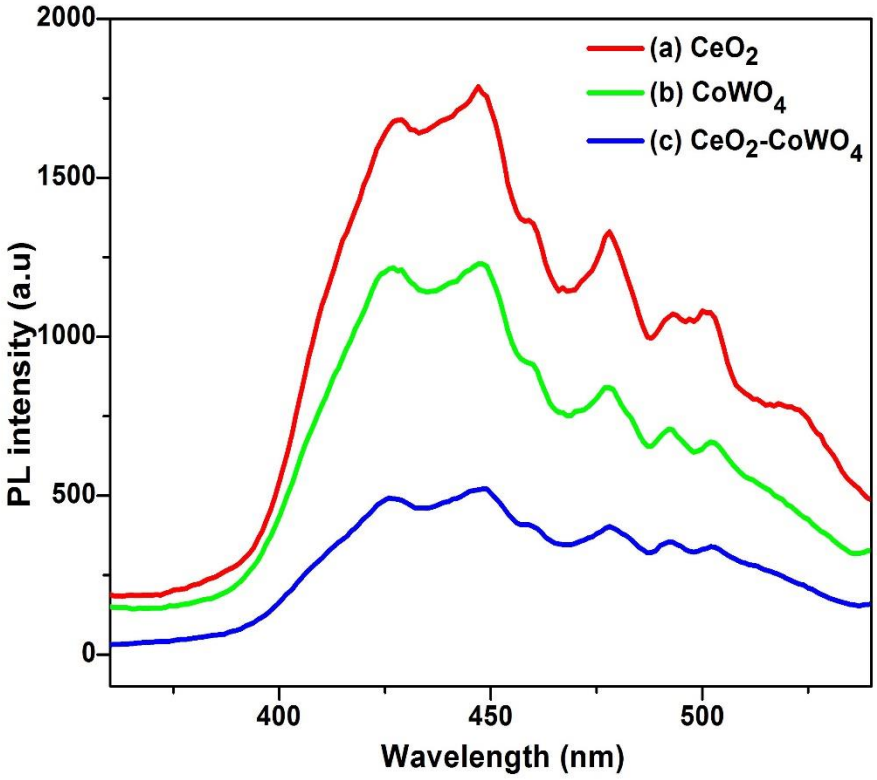
2000
1500
1000
500
0
PL intensity (a.u)
400
450
500
Wavelength (nm)
(a) CeO2
(b) CoWO4
(c) CeO2-CoWO4

Fig. 7

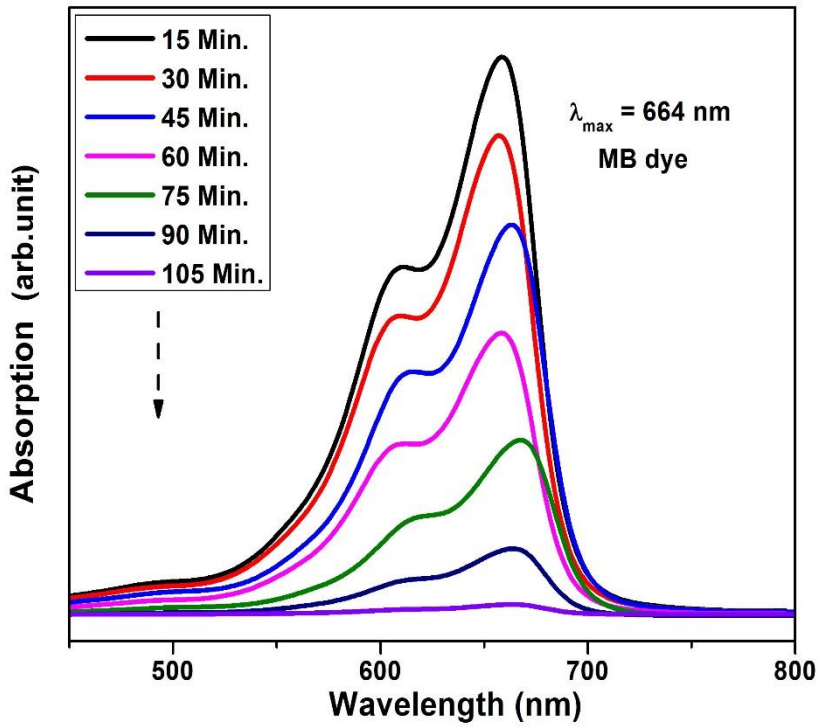
15 Min.
30 Min.
45 Min.
60 Min.
75 Min.
90 Min.
105 Min.
λmax = 664 nm
MB dye
Absorption (arb.unit)
500
600
700
800
Wavelength (nm)

**Fig. 8**

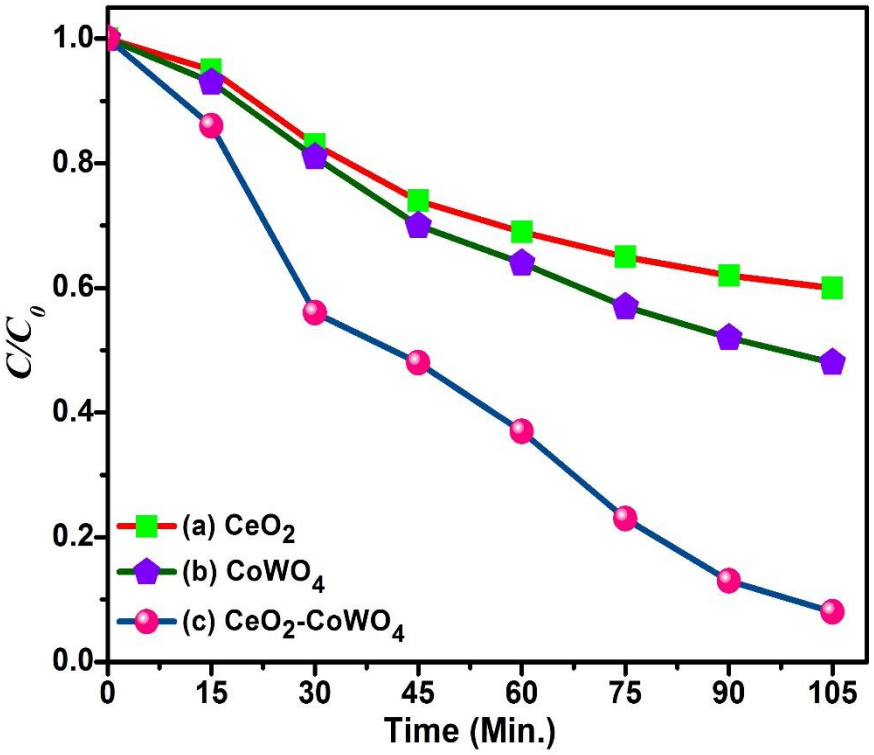
1.0
0.8
0.6
0.4
0.2
0.0
C/C0
0
15
30
45
60
75
90
105
Time (Min.)
(a) CeO2
(b) CoWO4
(c) CeO2-CoWO4

**Fig. 9**

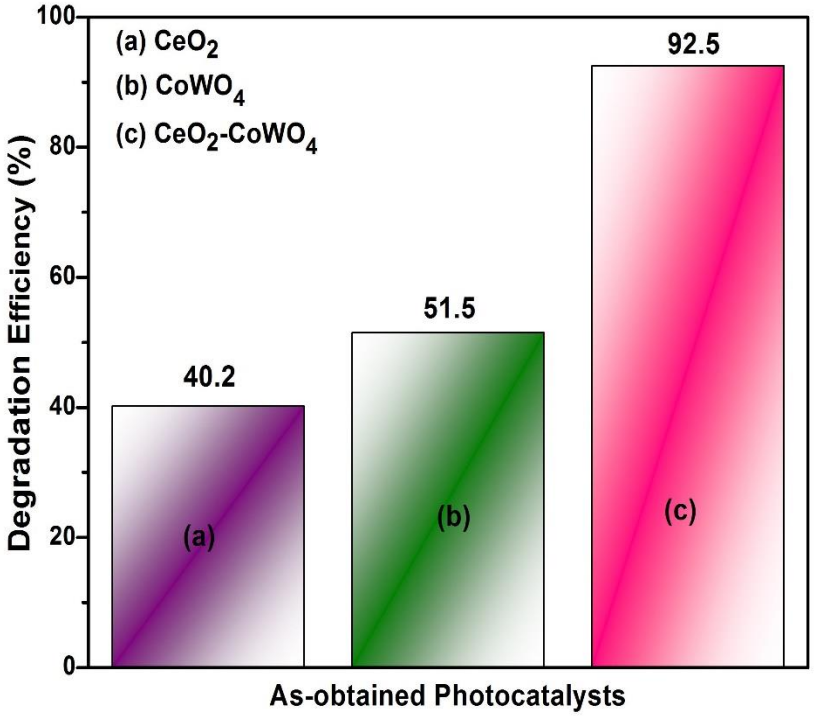
(a) CeO2
(b) CoWO4
(c) CeO2-CoWO4
Degradation Efficiency (%)
100
80
60
40
20
0
40.2
51.5
92.5
(a)
(b)
(c)
As-obtained Photocatalysts

**Fig. 10**

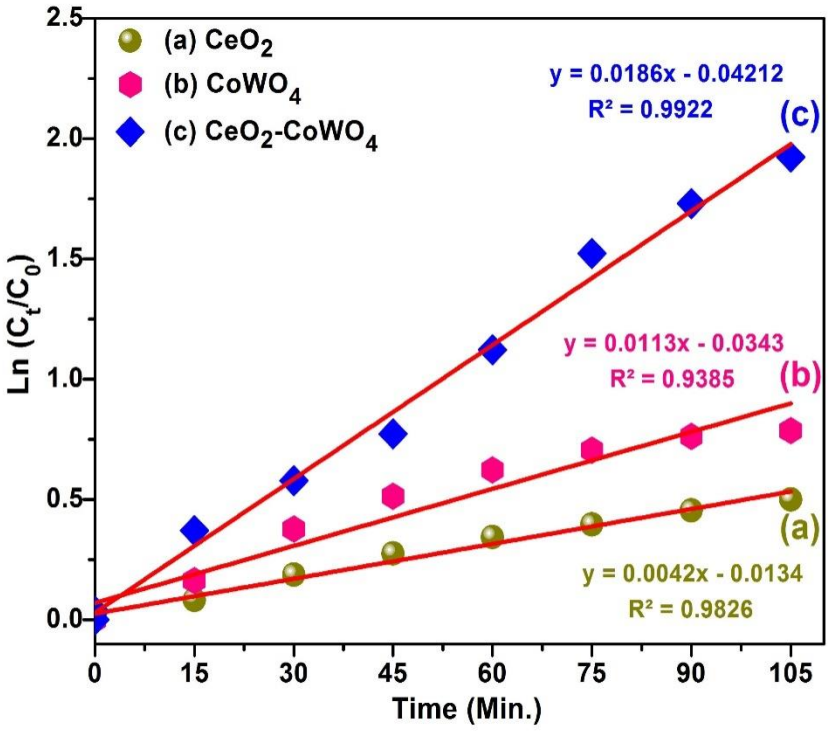
(a) CeO2
(b) CoWO4
(c) CeO2-CoWO4
y = 0.0186x - 0.04212
R² = 0.9922
(c)
y = 0.0113x - 0.0343
R² = 0.9385
(b)
(a)
y = 0.0042x - 0.0134
R² = 0.9826
Ln (Ct/C0)
Time (Min.)
0.0
0.5
1.0
1.5
2.0
2.5
0
15
30
45
60
75
90
105

**Fig. 11**

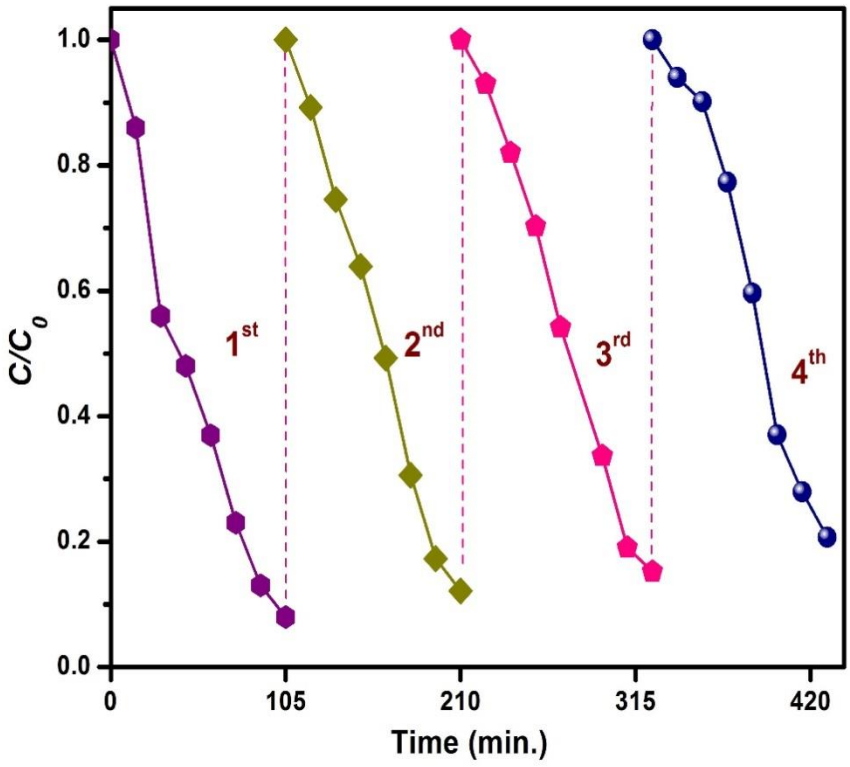


**Fig. 12**

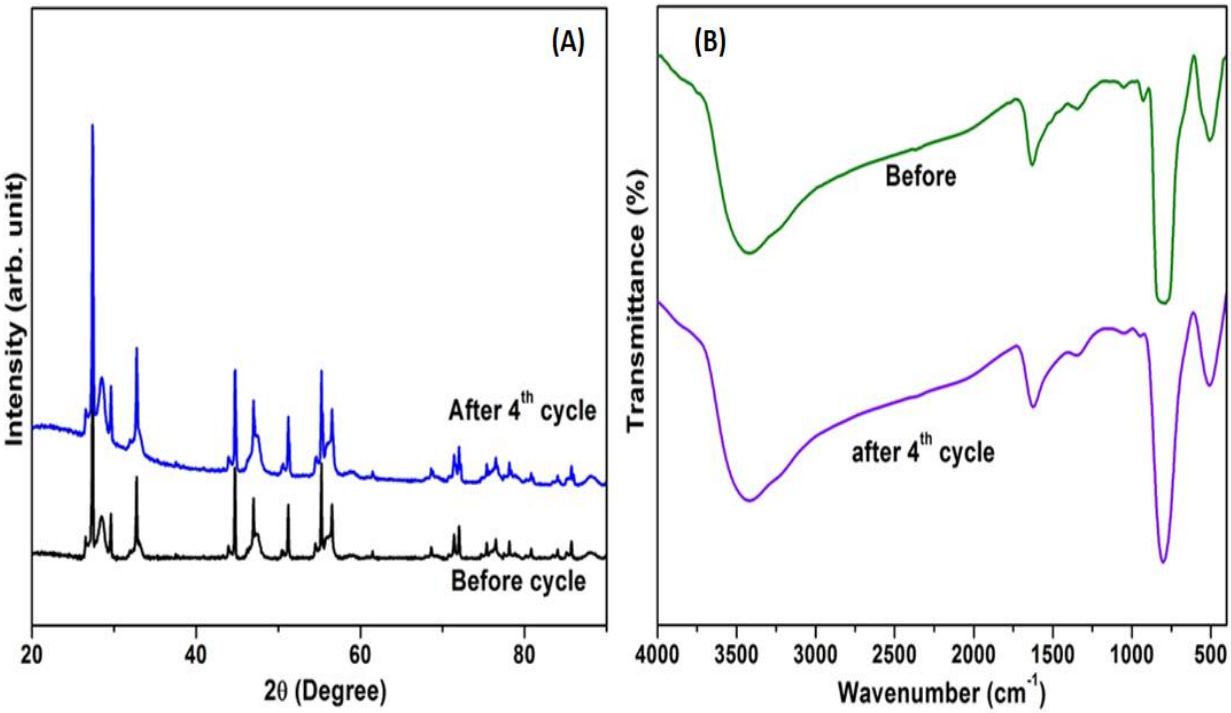
(A)
Intensity (arb. unit)
After 4th cycle
Before cycle
20
40
60
80
2θ (Degree)
(B)
Transmittance (%)
Before
after 4th cycle
4000
3500
3000
2500
2000
1500
1000
500
Wavenumber (cm-1)

**Fig. 13**

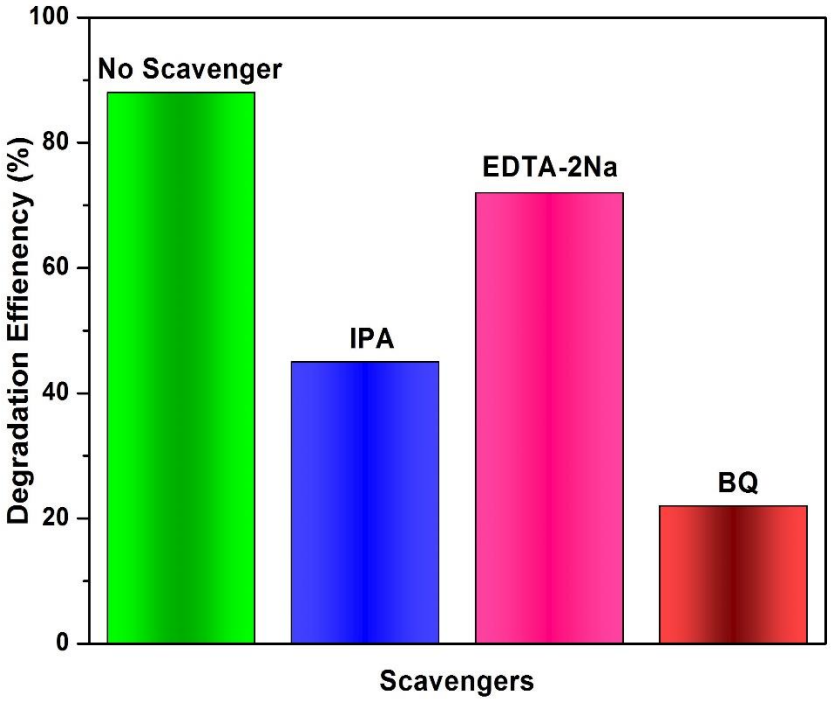
100
80
60
40
20
0
Degradation Effienency (%)
No Scavenger
IPA
EDTA-2Na
BQ
Scavengers

**Fig. 14**

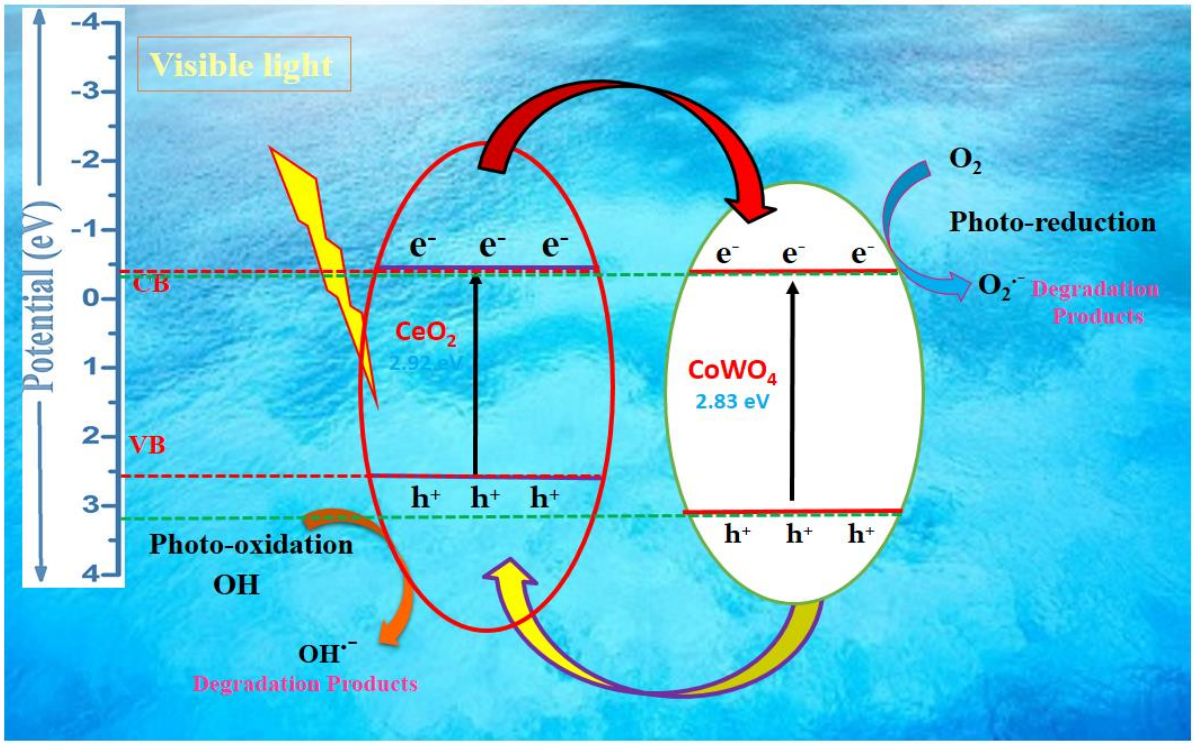
Potential (eV)
-4
-3
-2
-1
0
1
2
3
4
Visible light
CB
VB
e⁻ e⁻ e⁻
h⁺ h⁺ h⁺
CeO2
2.92 eV
CoWO4
2.83 eV
O2
Photo-reduction
O2•⁻
Degradation Products
Photo-oxidation
OH
OH•⁻
Degradation Products

**Fig. 15**

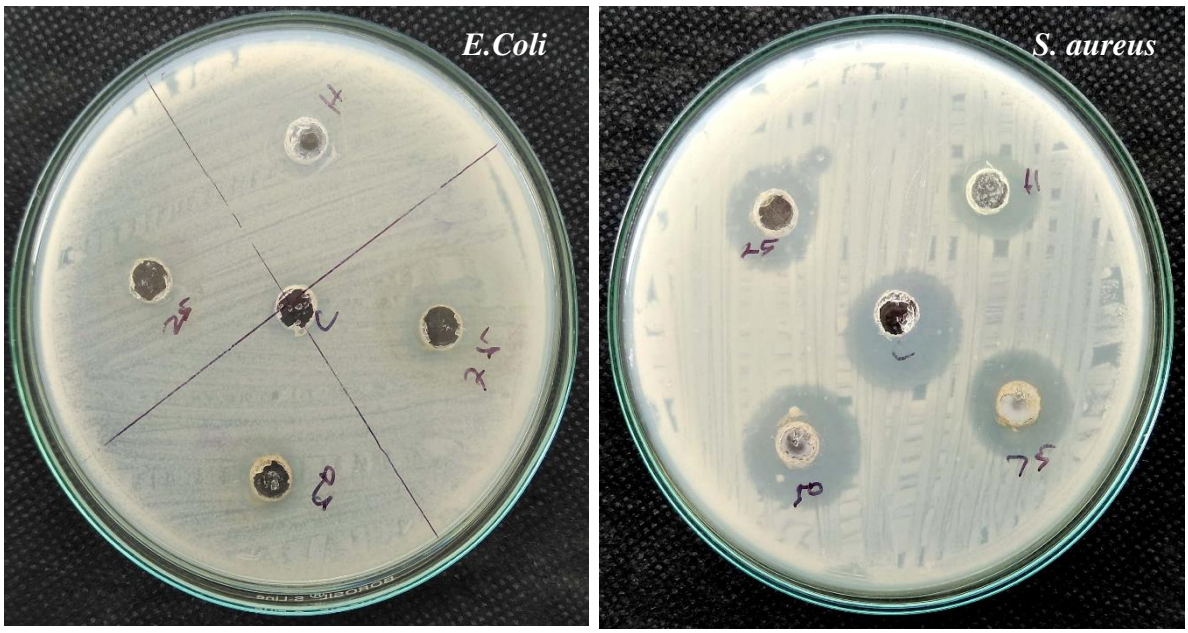


**Fig. 16**

# Figures

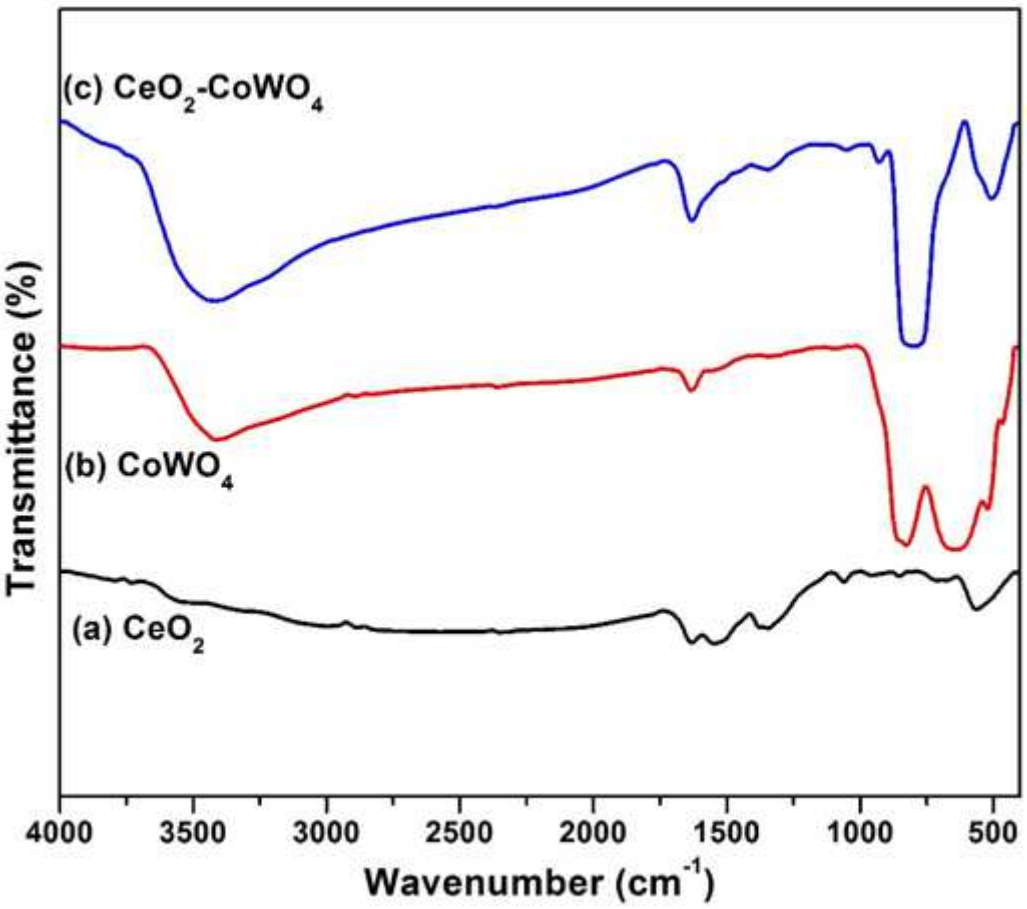


**Figure 1**

XRD pattern of (a) CeO2 (b) CoWO4 and (c) CeO2/CoWO4 NCs

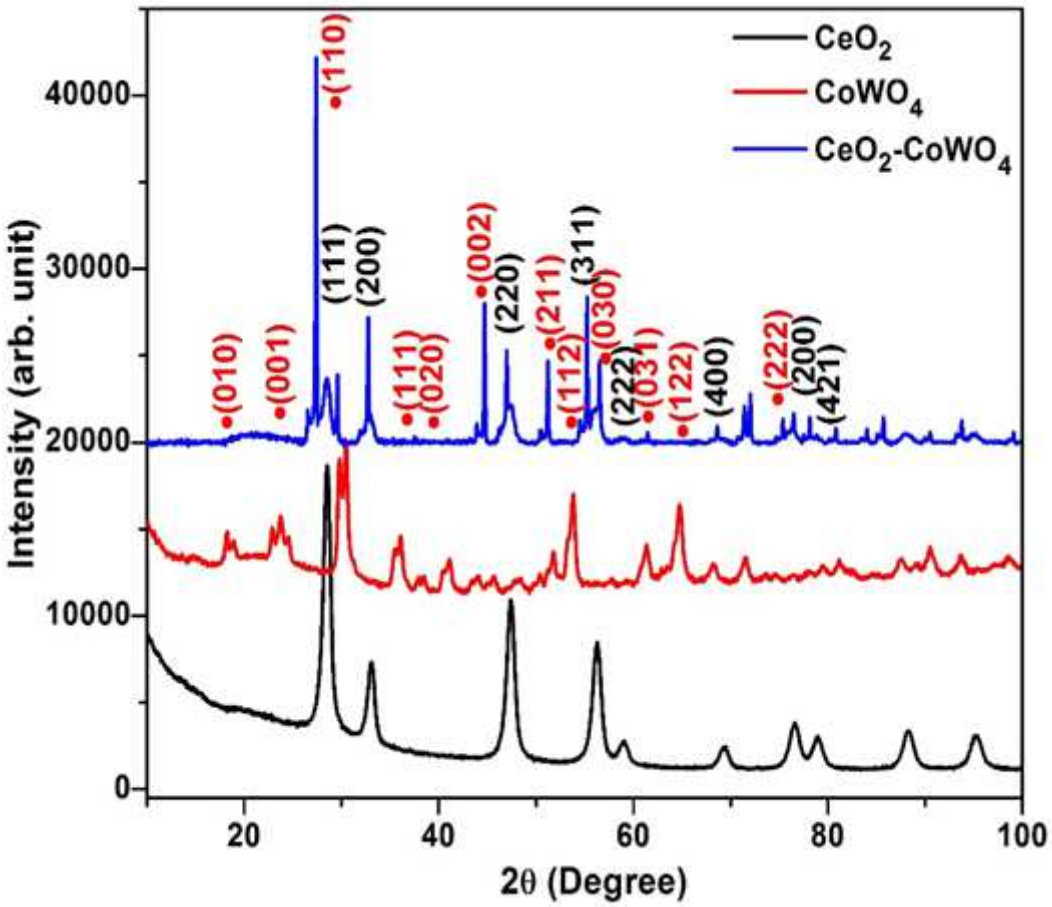


**Figure 2**

FTIR spectra of (a) CeO2 (b) CoWO4 and (c) CeO2/CoWO4 NCs

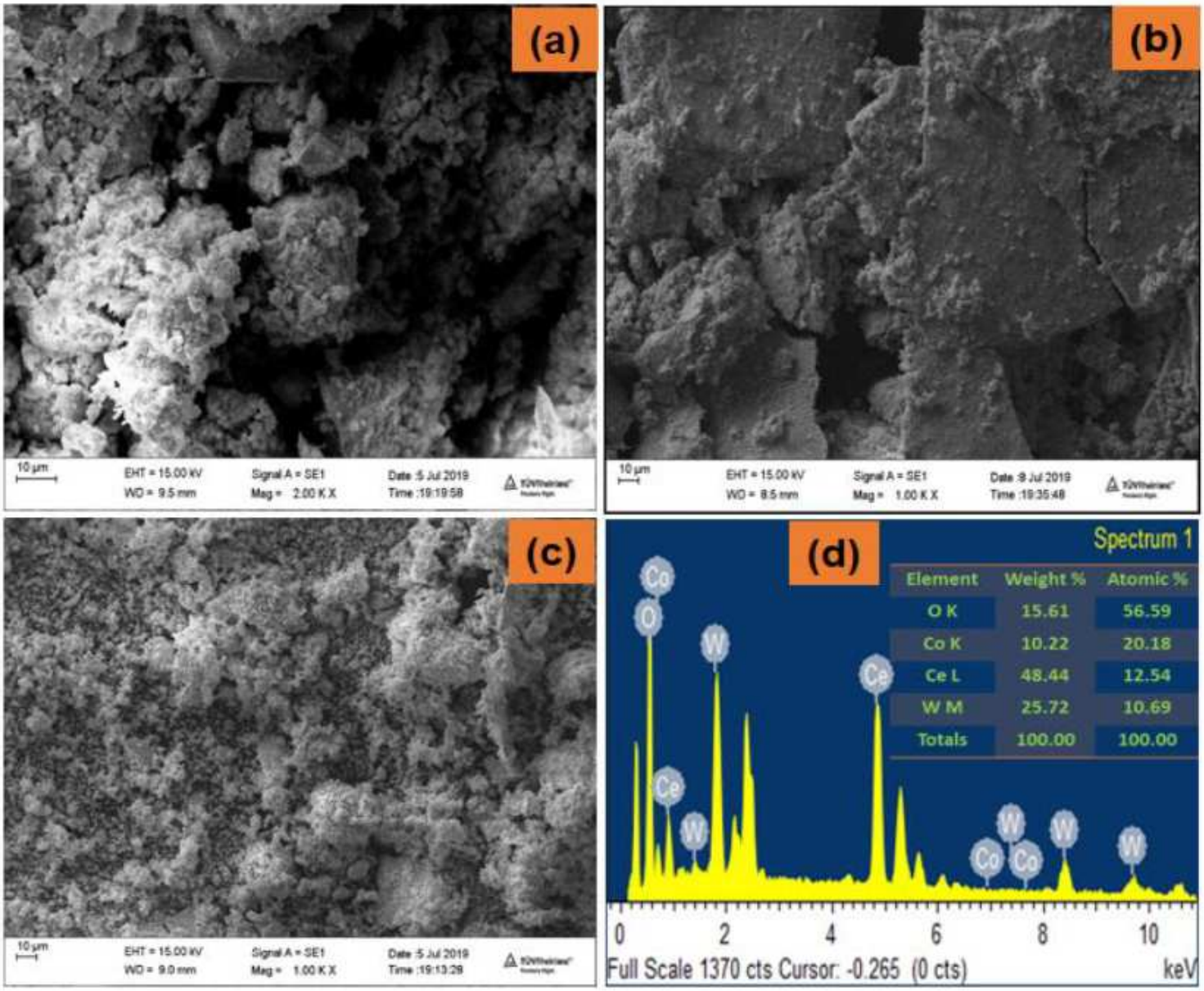


## Figure 3

HR-SEM images of (a) CeO2 (b) CoWO4 (c) CeO2/CoWO4 and (d) EDAX spectra of CeO2/CoWO4 NCs

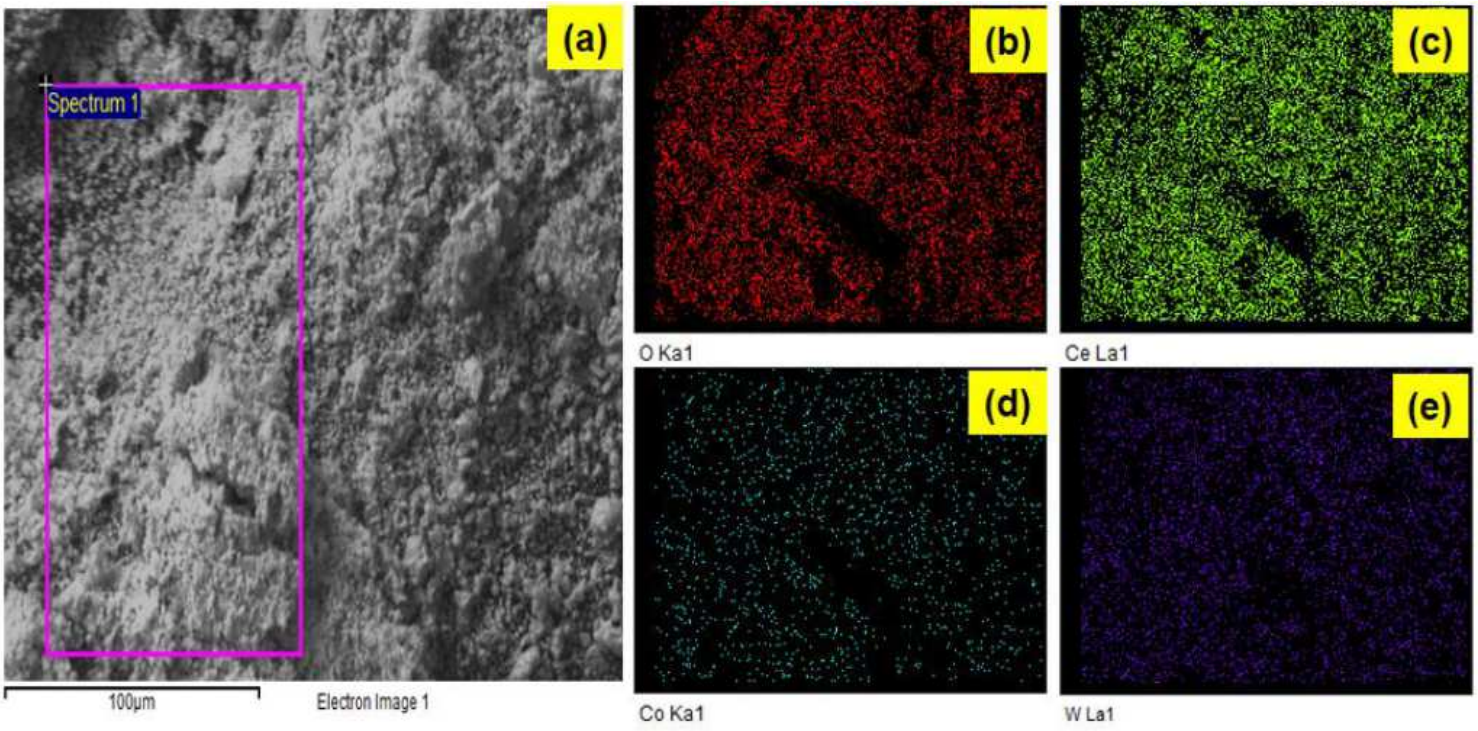


**Figure 4**

Elemental mapping of CeO2/CoWO4 NCs

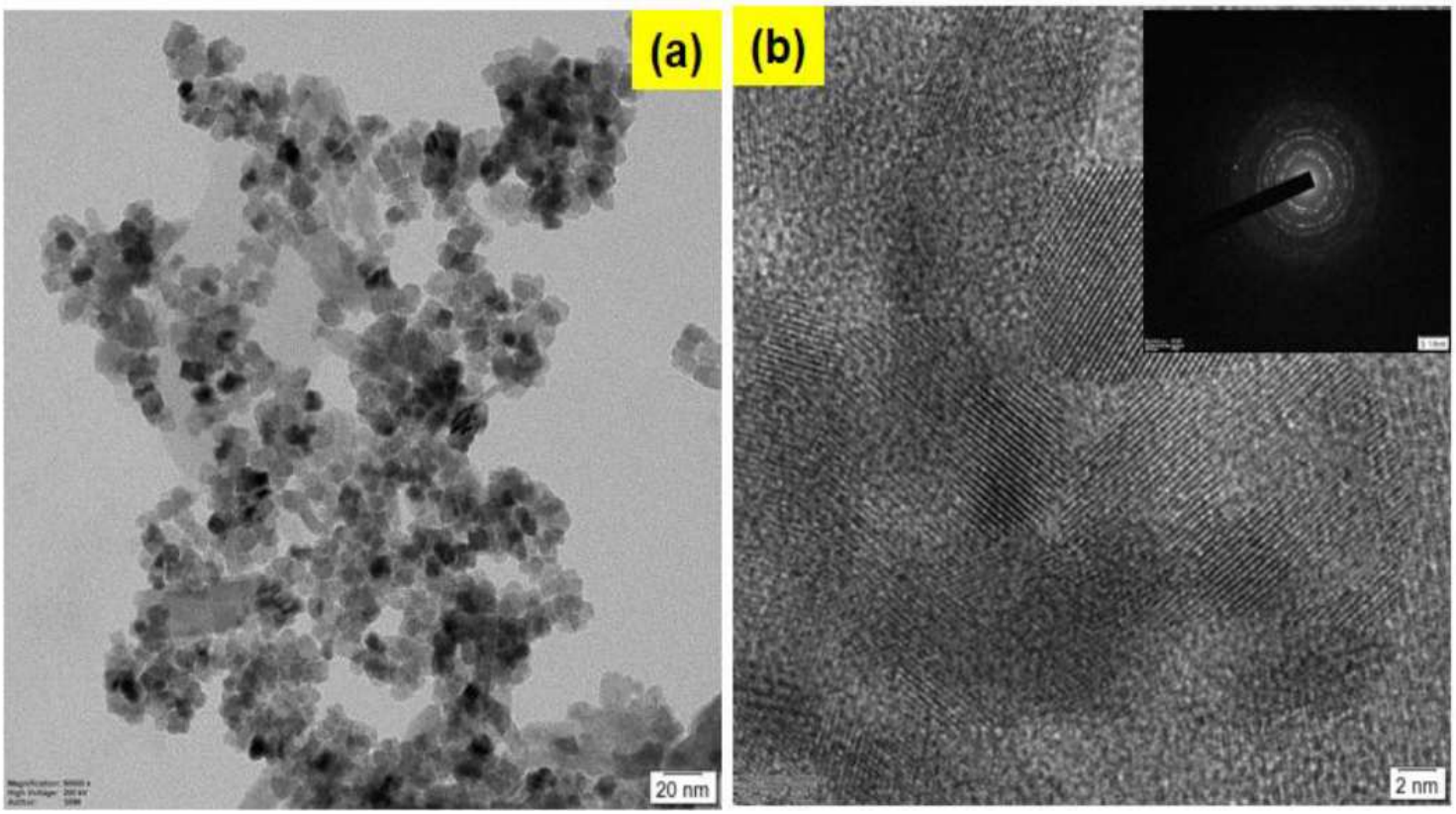


**Figure 5**

HR-TEM images of as-obtained CeO2/CoWO4 NCs

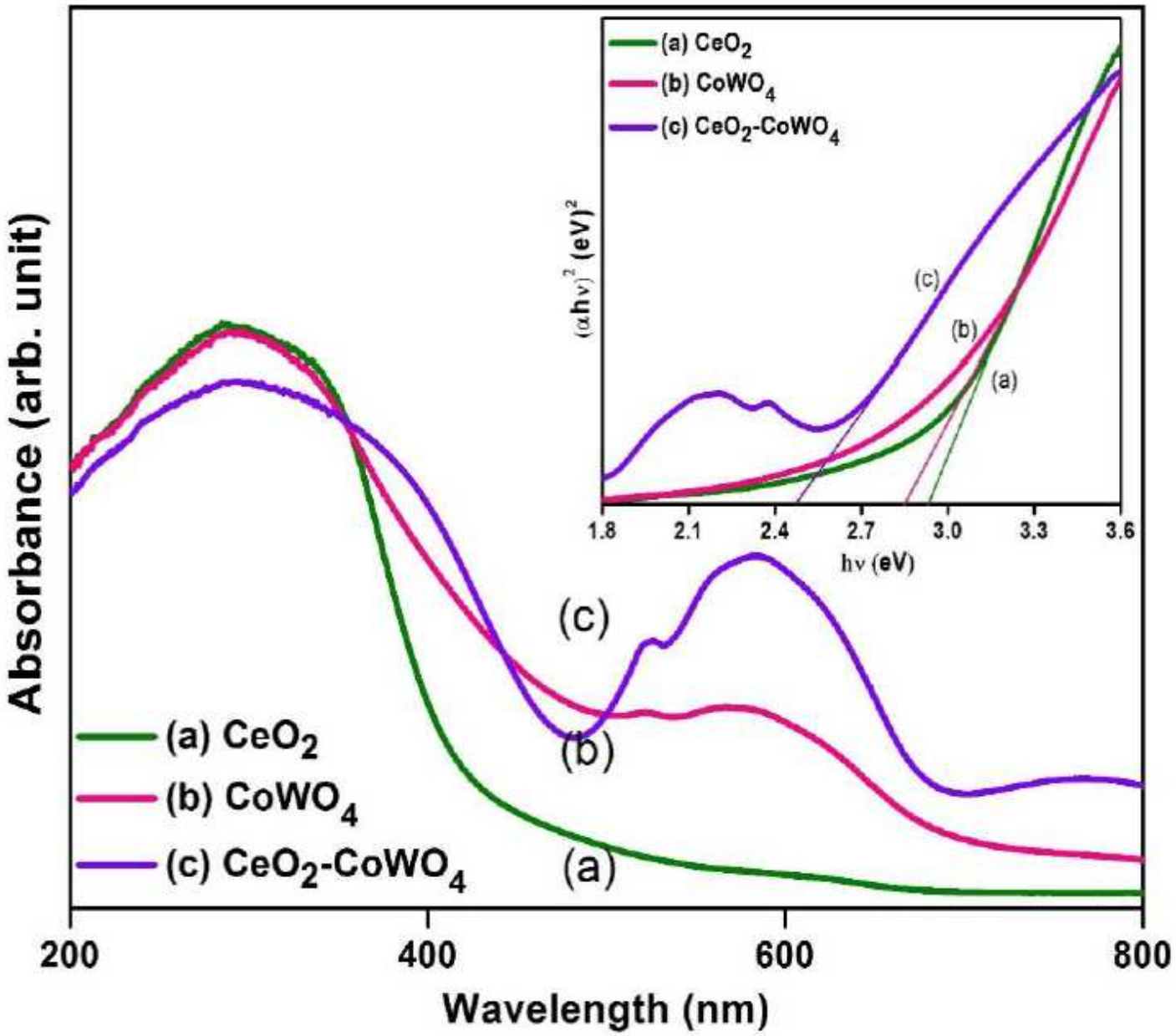


Figure 6

UV-Vis DRS spectra and (inset) Band gap energy of as-obtained nanomaterials

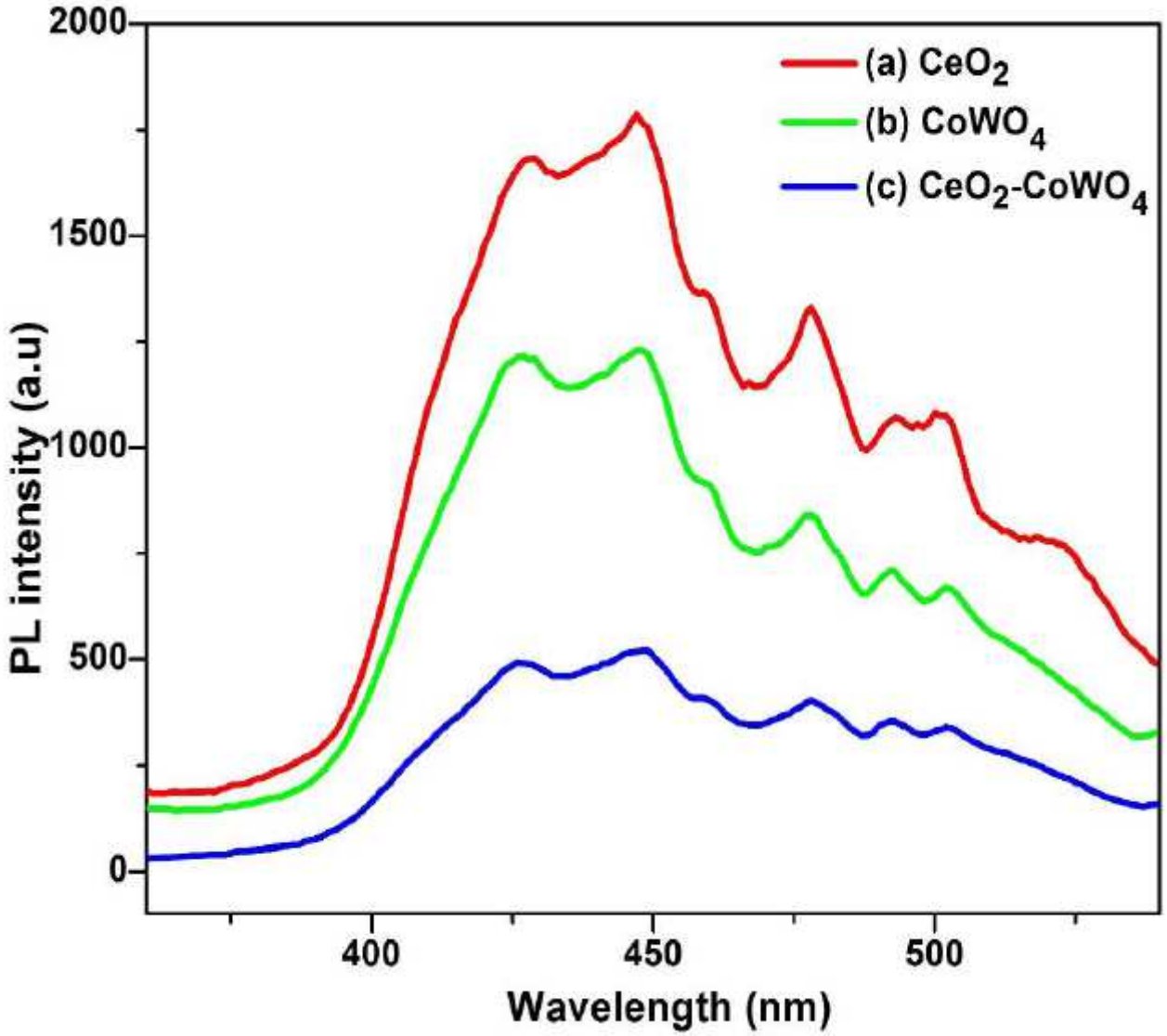


**Figure 7**

Room-temperature PL spectra of as-obtained nanomaterials

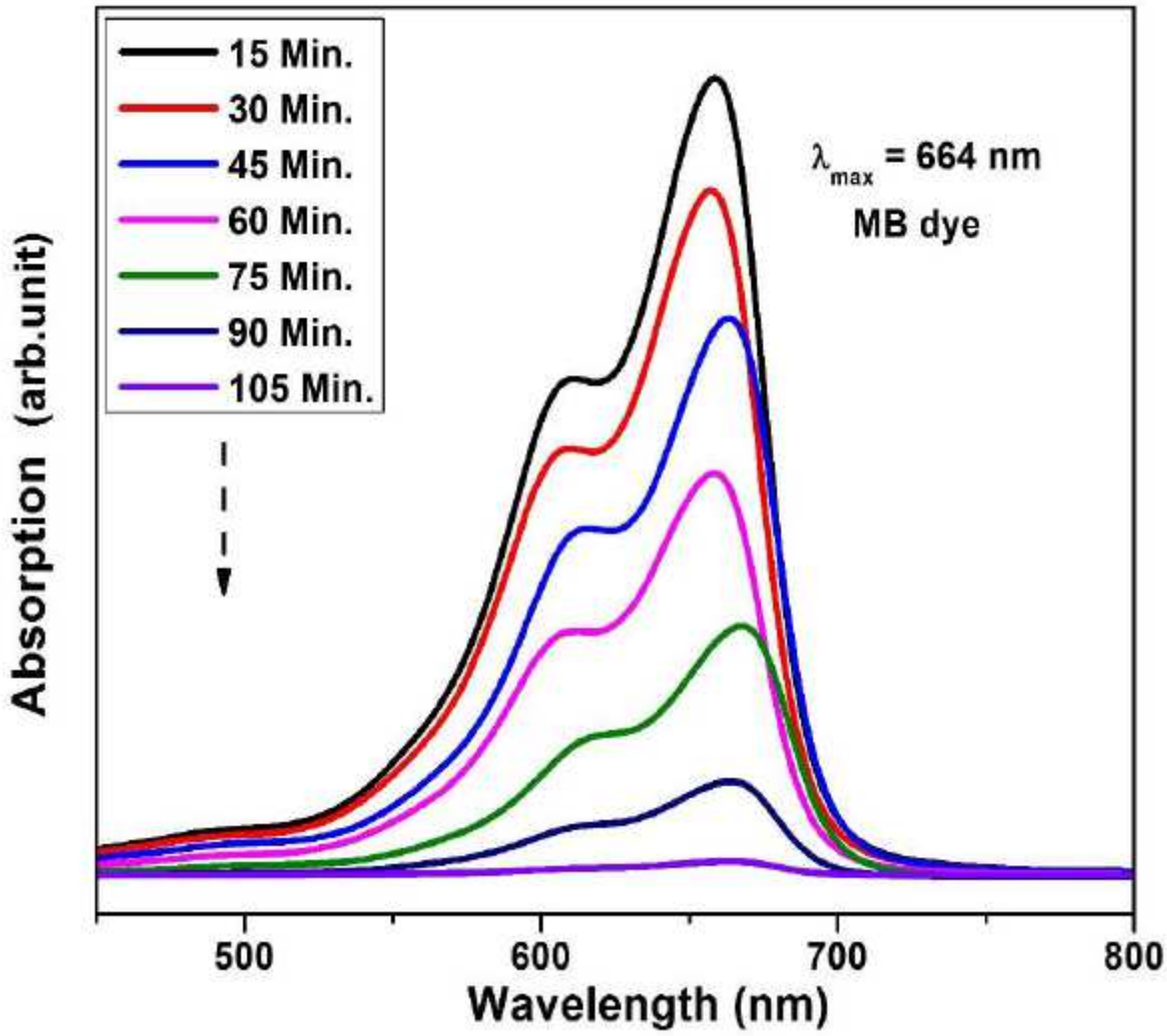


**Figure 8**

UV-Vis absorption spectra of MB dye degradation of CeO2/CoWO4 NCs

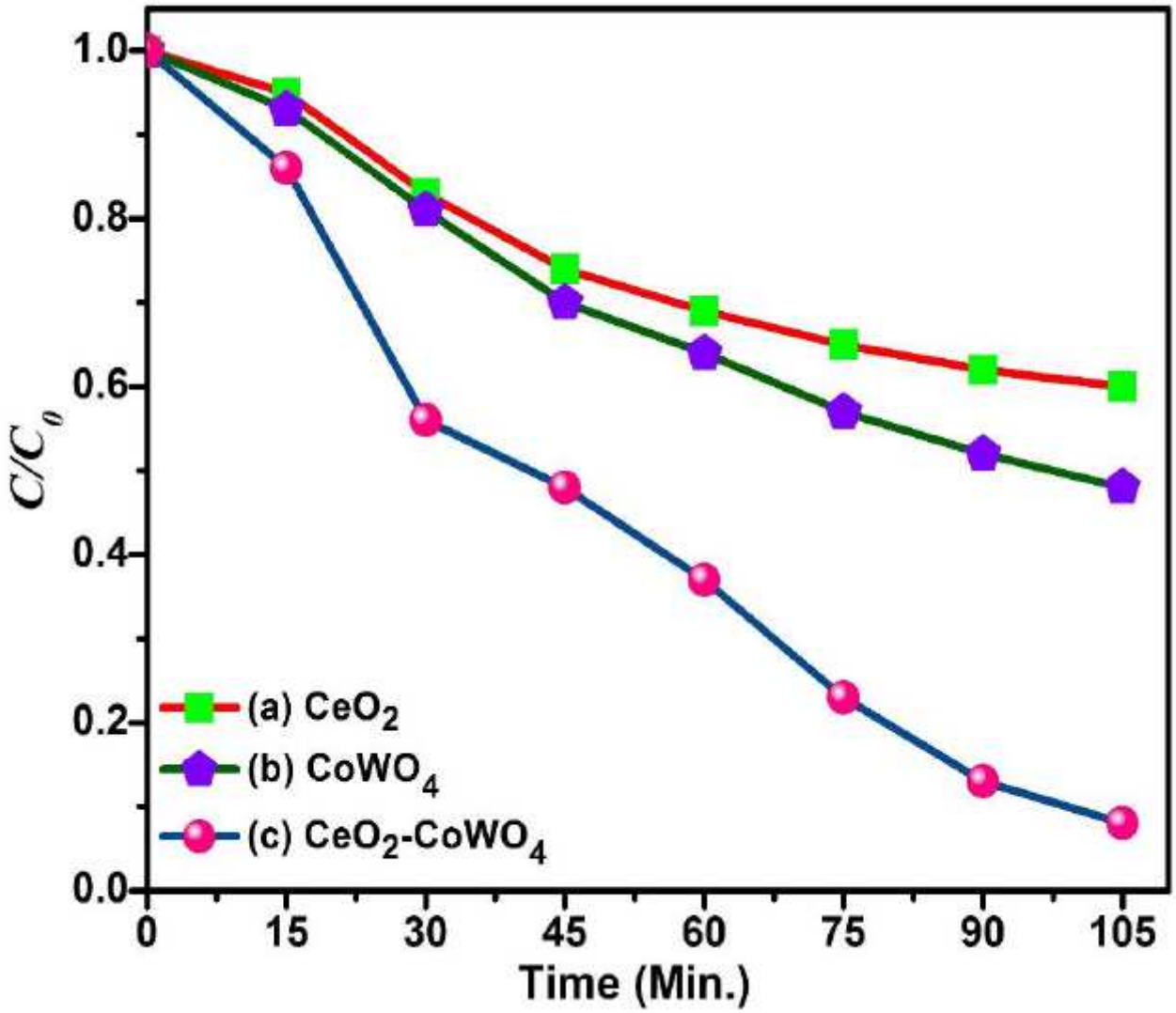


**Figure 9**

Photodegradation of MB dye over the (a) CeO2 (b) CoWO4 (c) CeO2/CoWO4 PCs

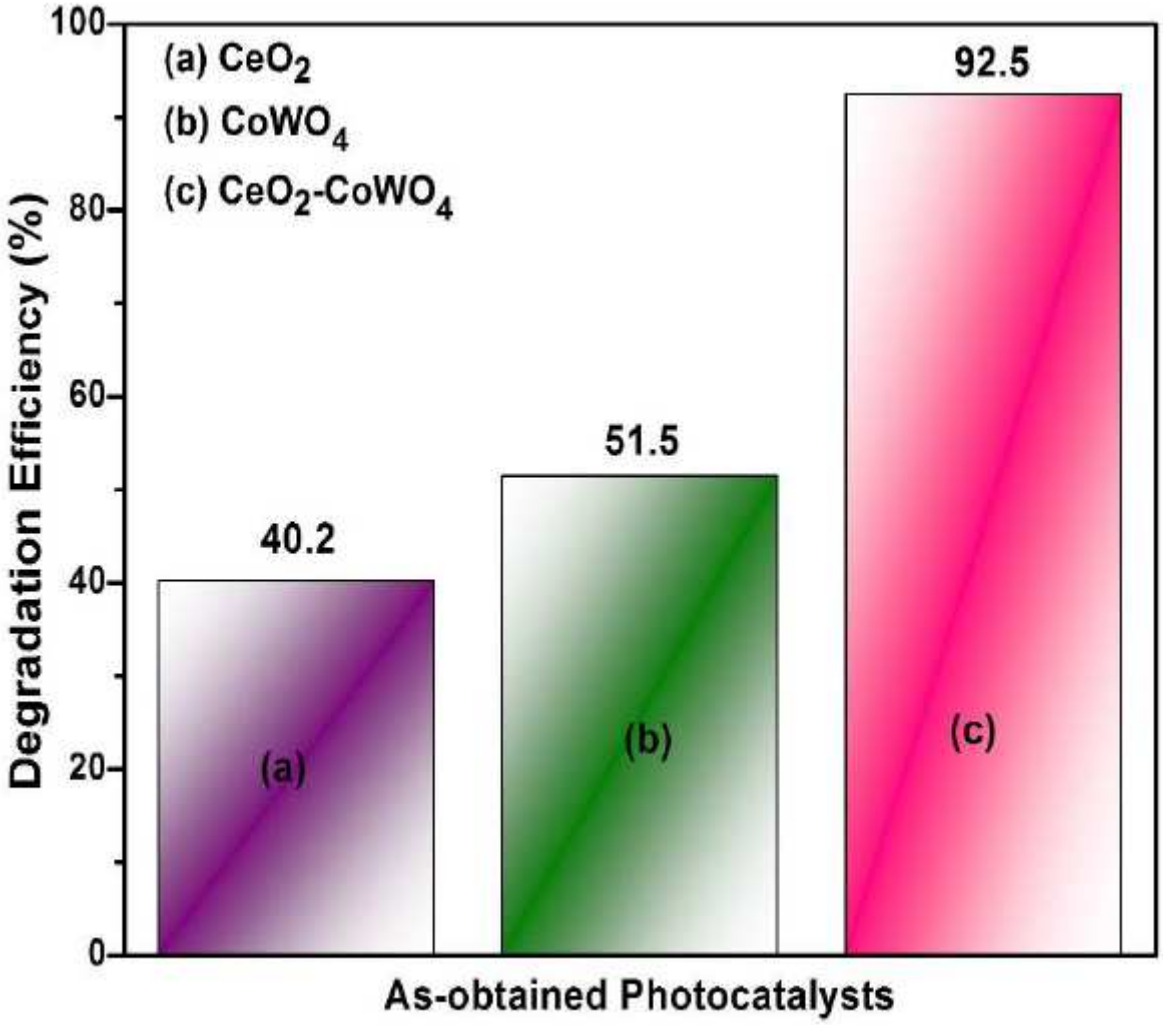


**Figure 10**

Degradation efficiency of MB dye by (a) CeO2 (b) CoWO4 (c) CeO2/CoWO4 PCs

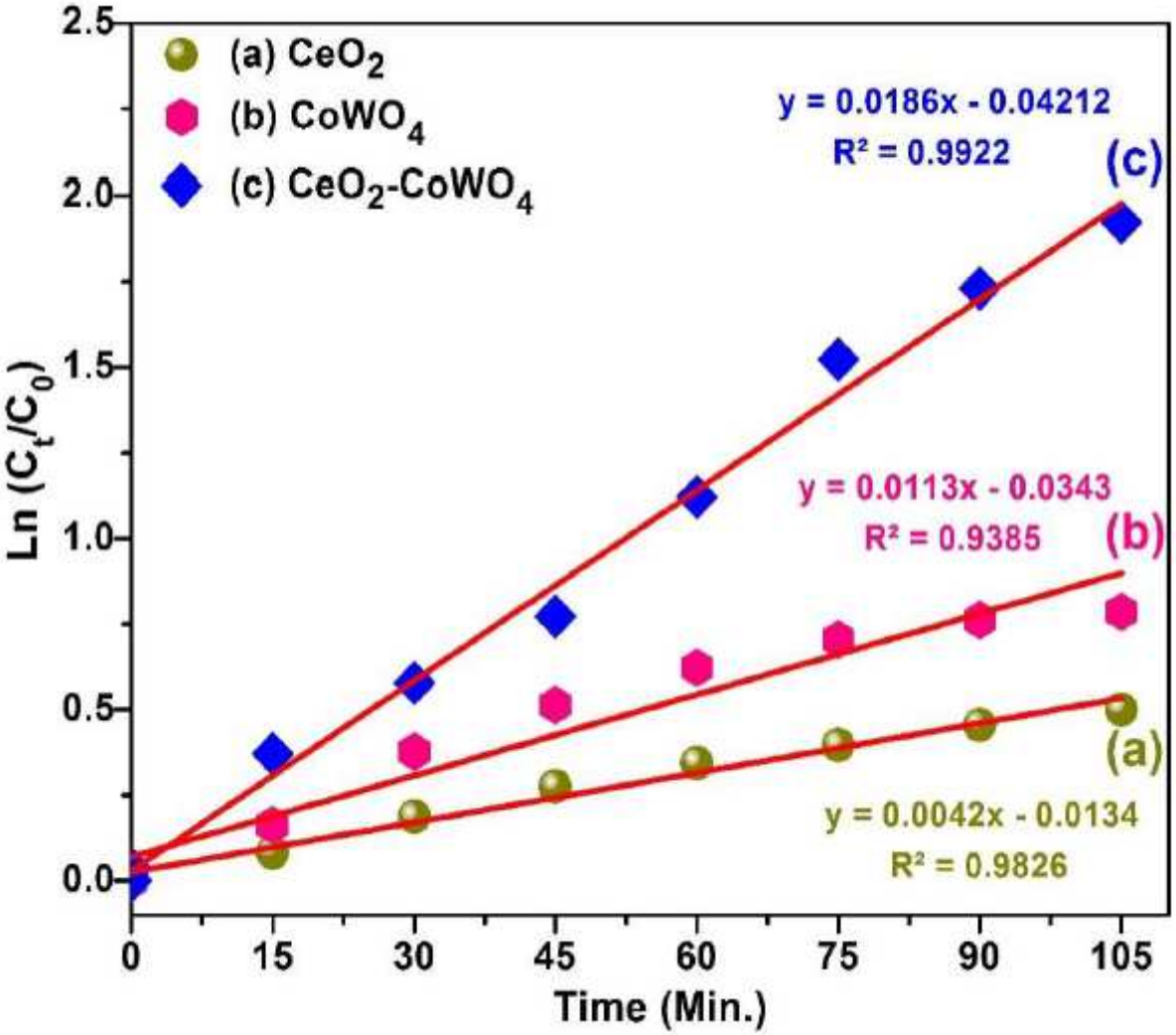


**Figure 11**

First-order kinetic plot for the degradation of MB over the as-obtained PCs

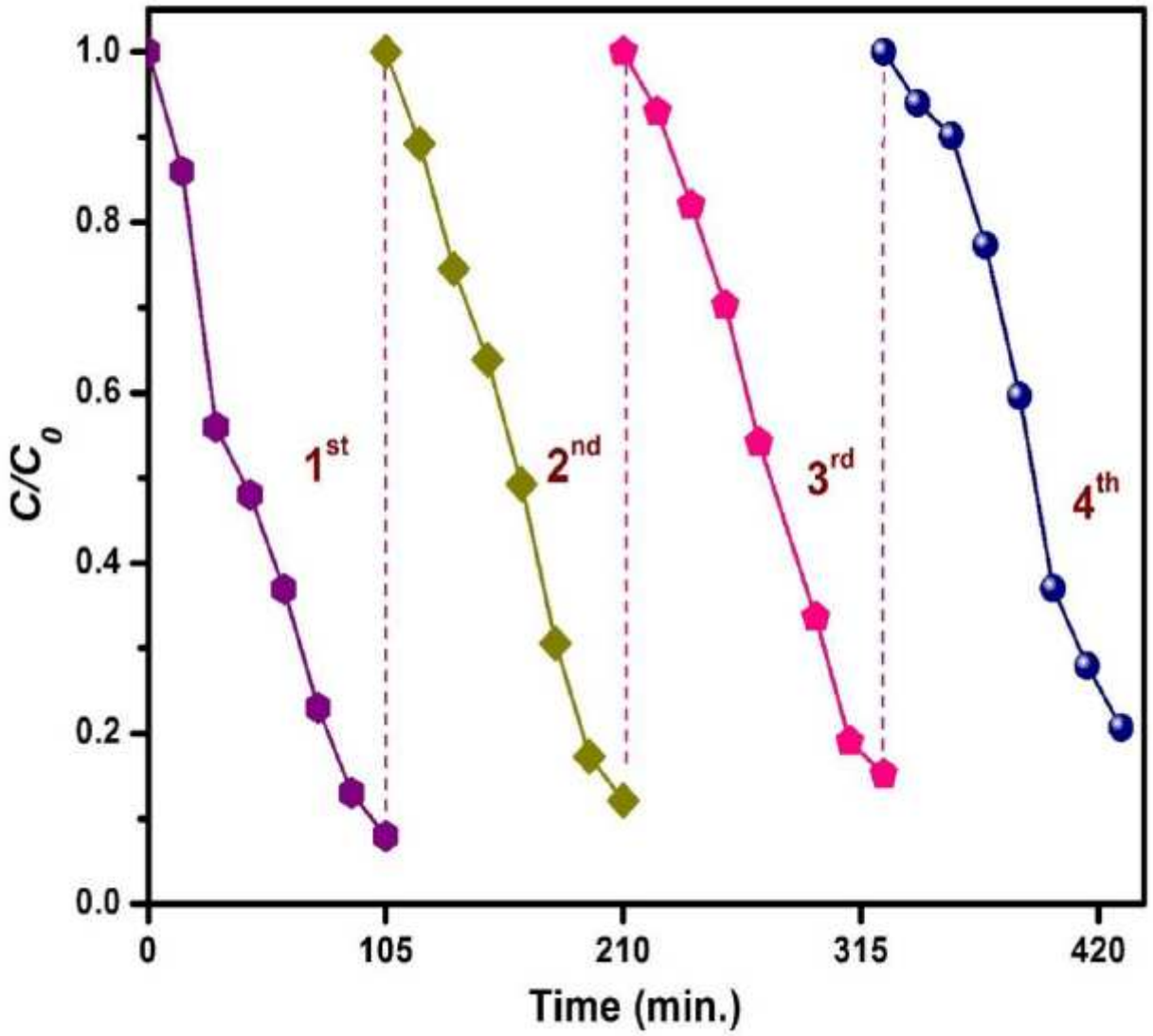


**Figure 12**

Four repetitive recycling processes of CeO2/CoWO4 PCs for photodegradation of MB dye under visible light exposure

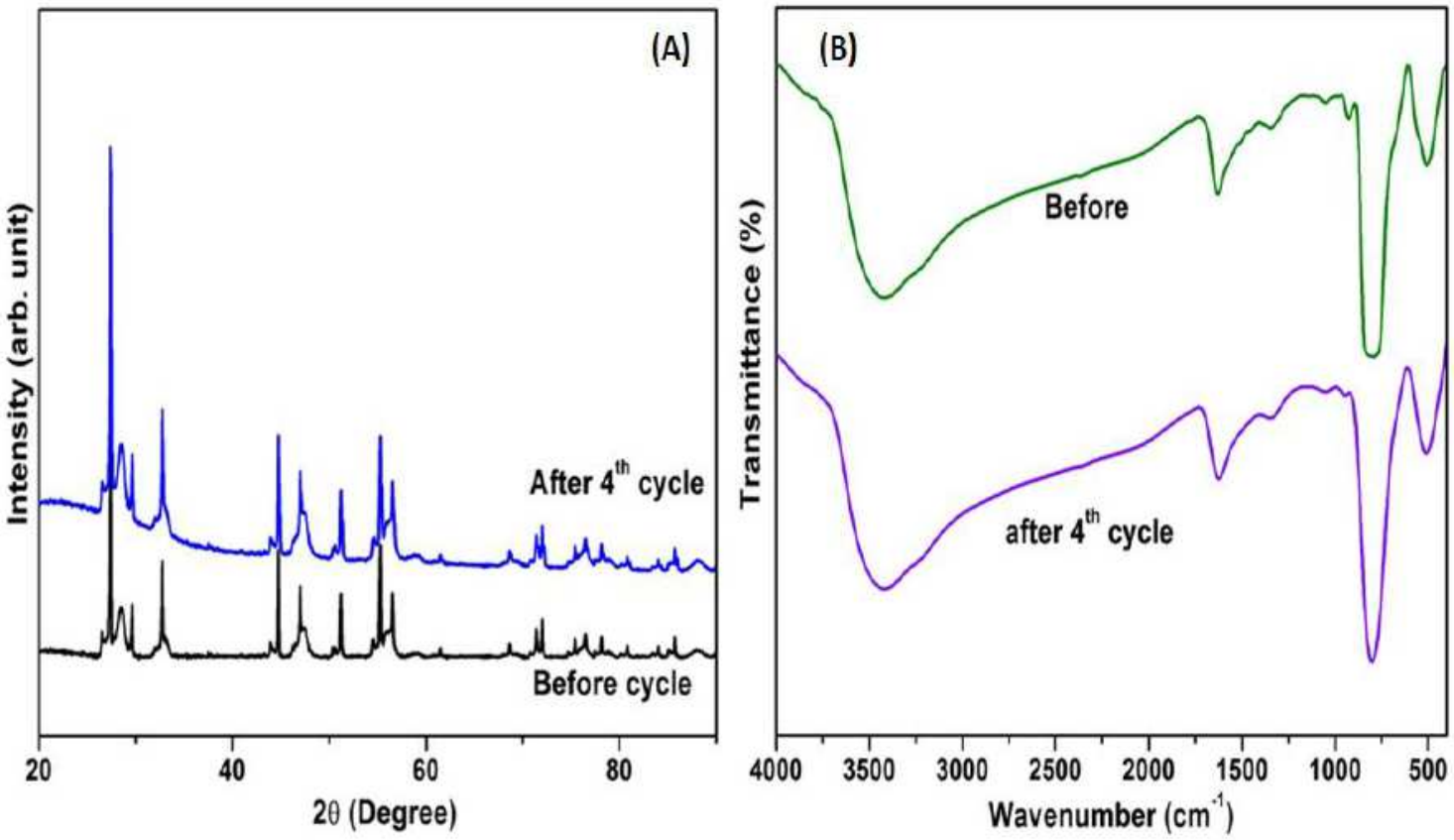


**Figure 13**

(A) XRD pattern and (B) FTIR spectra for CeO2/CoWO4 PCs before and after a photocatalytic reaction

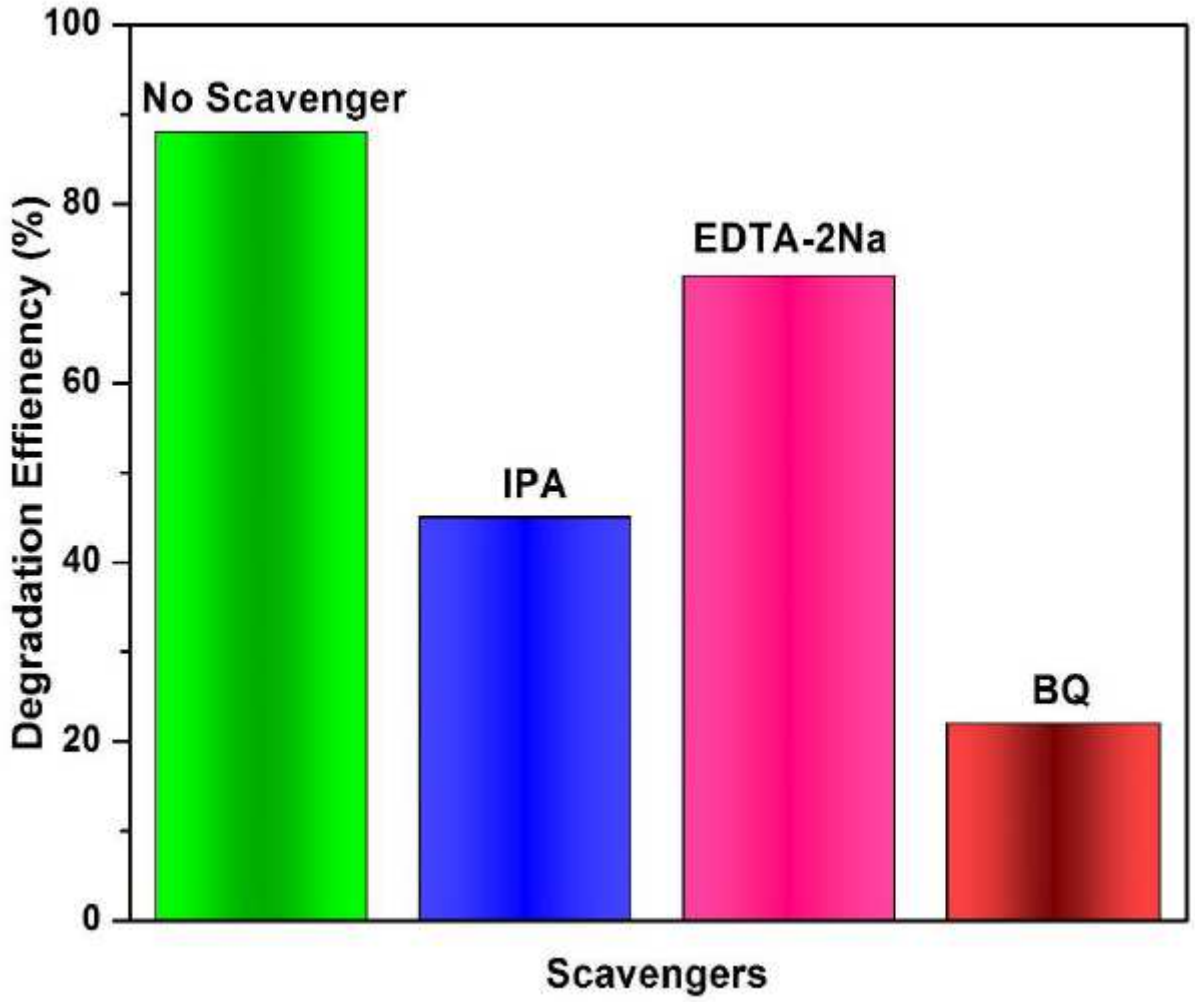


**Figure 14**

Effects of different scavengers on the degradation of MB dye in the presence of CeO2/CoWO4 PCs

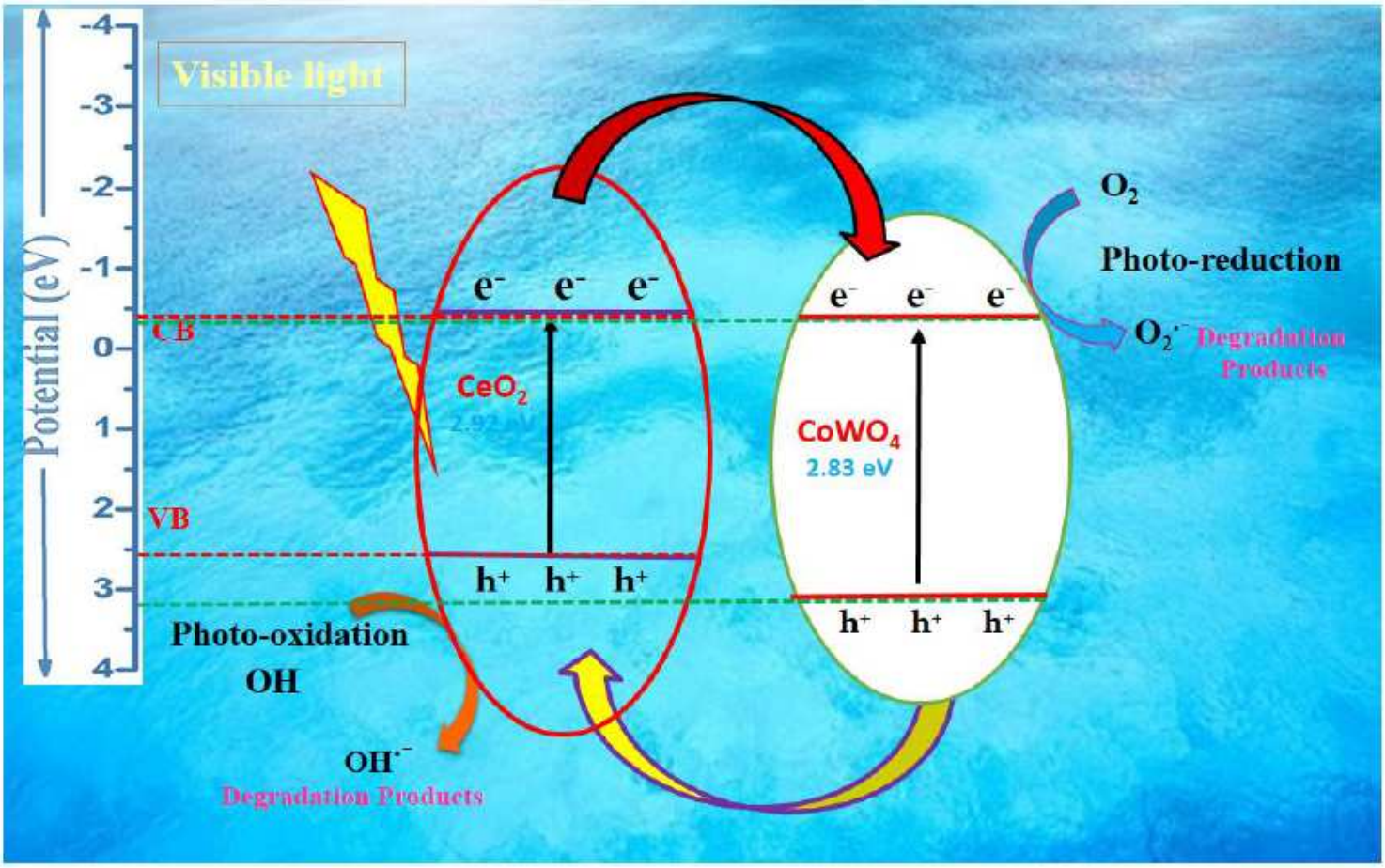


Figure 15

The plausible mechanism of the MB dye degradation for CeO2/CoWO4 PCs

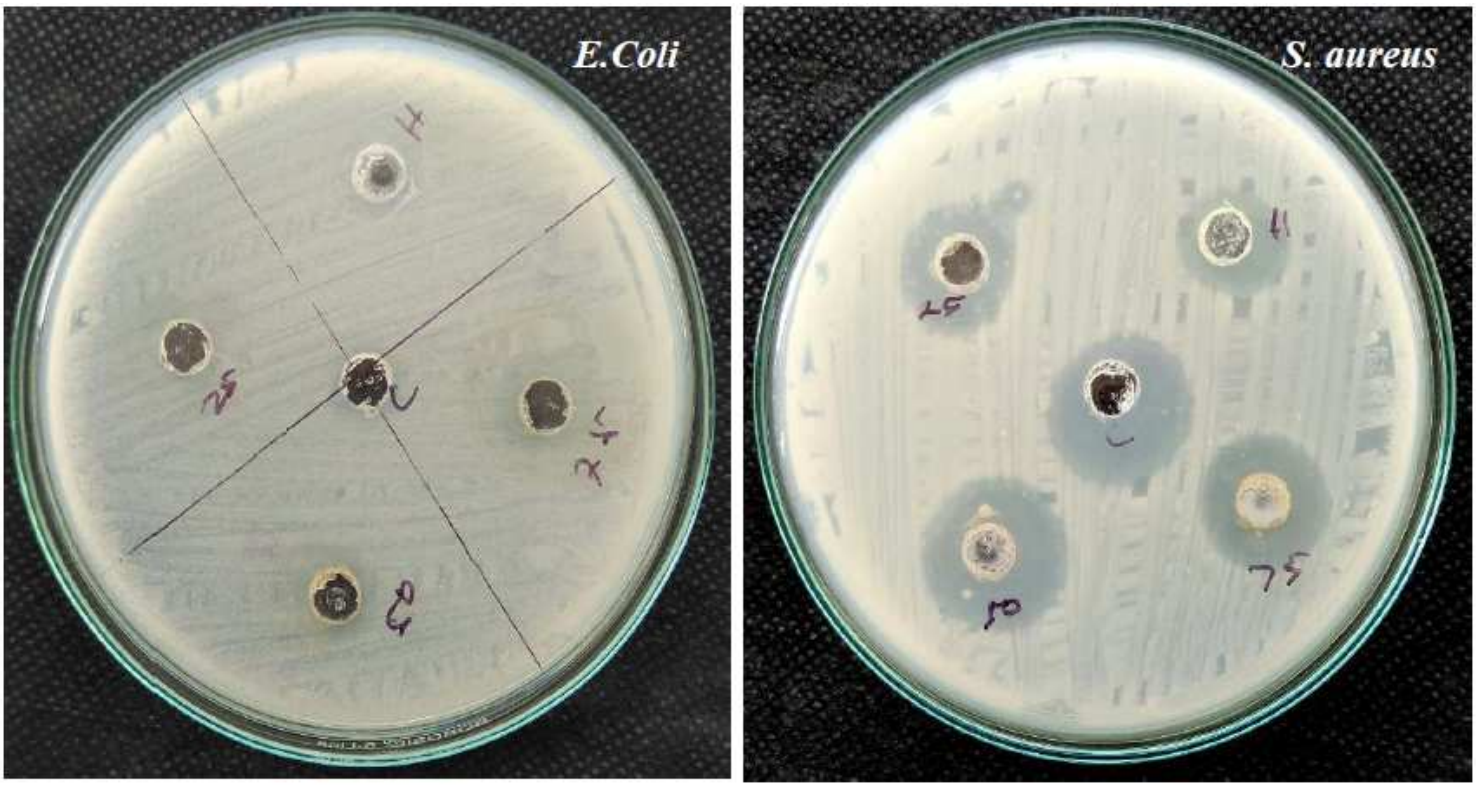

## Figure 16

Antibacterial ZOI value by (G-) E. coli and (G+) of S. aureus bacteria of 75 µg as-prepared CeO2/CoWO4 nanomaterials